Designing Low-PAPR Waveform for OFDM-based RadCom Systems

Yixuan Huang, Su Hu, Shiyong Ma, Zilong Liu and Ming Xiao

***Abstract*— This paper is focused on the fusion of radar and wireless communication, called RadCom, which has been extensively studied in recent years for future intelligent transportation systems. We propose a new waveform design algorithm for reducing peak-to-average power ratio (PAPR) in OFDM-based RadCom systems. We consider a flexible and generic RadCom structure in which a number of non-contiguous sub-bands for data transmission are located within a large contiguous spectrum band for radar detection/sensing. New RadCom waveforms with low PAPR are obtained by carrying out optimization over those subcarriers which are complementary to the communication bands. As an application of the majorization-minimization (MM) optimization method, our major contribution is an l-norm cyclic algorithm which is capable of efficiently reducing the maximum PAPR of RadCom waveforms. We show by numerical simulation results that significant performance enhancements can be achieved compared to OFDM RadCom waveforms from legacy approaches.**

***Index Terms*—RadCom, Peak-to-Average Power Ratio (PAPR), Orthogonal Frequency-Division Multiplexing (OFDM), Waveform Design, Internet-of-Vehicles (IoV).**

I. Introduction

THE safety and user experiences of drivers and passengers are vital in vehicular field. Both the communication and radar functions are becoming increasingly indispensable in a modern car. While the former is used for information exchange, the latter is key for the prevention of any potential traffic hazards and/or collisions. Since both the communication and radar systems bear certain similarities with respect to the system structure and signal processing algorithms, an emerging trend is to integrate these two into one, where the resultant system is called "RadCom" [1] or joint radar-communications (JRC) [2] for internet-of-vehicles (IoV) and autonomous driving so as to attain a number of benefits such as low hardware cost and high spectrum efficiency. Specifically, the radar sensing/detection precision may be improved based on the feedback from the communication module which potentially carries certain key driving information, such as the geographical locations, moving speeds, and planned driving routes. The outputs of the radar module can also help improve the performances of the communication counterpart, for example, by adjusting the antenna position to facilitate direction-sensitive signal processing (such as beamforming) and/or adjusting the coding rates and modulation schemes based on the estimated distances/speeds of vehicles to meet a vast range of quality-of-service requirements. In Fig. 1, four vehicles exchange different types of vehicular information with the aid of RadCom waveforms while the targets, such as neighboring vehicles, pedestrians, or road-side units, are captured simultaneously by an in-car RadCom equipment for enhancement of traffic safety.

A. Literature Review

Existing contributions on RadCom mainly focus on two aspects [3]: 1) co-existence of existing radar and communication devices and 2) co-design for dual-functional systems. One of the best candidates for RadCom is orthogonal frequency division multiplexing (OFDM), which has found applications in numerous communication systems/standards owing to their capabilities of efficient system implementation and high spectrum efficiency [1], [4]–[7]. With the total power constraint and based on information theory, an adaptive OFDM-based RadCom waveform design method has been devised in [8]. A robust OFDM radar waveform design has been introduced in a co-existence RadCom system by three power minimization criteria [9]. [1] studied an OFDM-based RadCom system, in which traditional communication OFDM is applied to capture target range and relative velocity in IoV scenarios by continuous wave (CW) radar processing[1]. An orthogonal frequency division multiple access (OFDMA) JRC system, including a bi-static automotive radar and IoV communications, has been investigated in [2]. To minimize the downlink multiuser interference with the total power constraint, [10] considers weighted optimizations for a flexible tradeoff between radar and communications performances in multi-input-multi-output (MIMO) RadCom beampattern design.

To attain excellent detection and communication performances in IoV scenarios, efficient design approaches of RadCom waveforms which not only enable high data rates but also possess good correlation characteristics (for radar sensing/detection) are desired [11]. The waveform autocorrelation property is of prime importance for ranging.

Y. Huang, S. Hu and S. Ma are with the National Key Laboratory on Communications, University of Electronic Science and Technology of China, Chengdu 611731, China. Corresponding author: Su Hu (e-mail: husu@uestc.edu.cn).

Z. Liu is with the School of Computer Science and Electronic Engineering, University of Essex, UK (email: zilong.liu@essex.ac.uk).

M. Xiao is with the Department of Information Science and Engineering, KTH Royal Institute of Technology, Stockholm 10044, Sweden (email: mingx@kth.se).

[1]Since all the subcarriers are employed for data transmission in [1], it is difficult to ensure a low PAPR. In comparison, this paper considers a generic RadCom structure that only a portion of certain contiguous frequency band is used for communication. This allows us to leverage the remaining frequency bands for PAPR reduction of the RadCom waveforms.

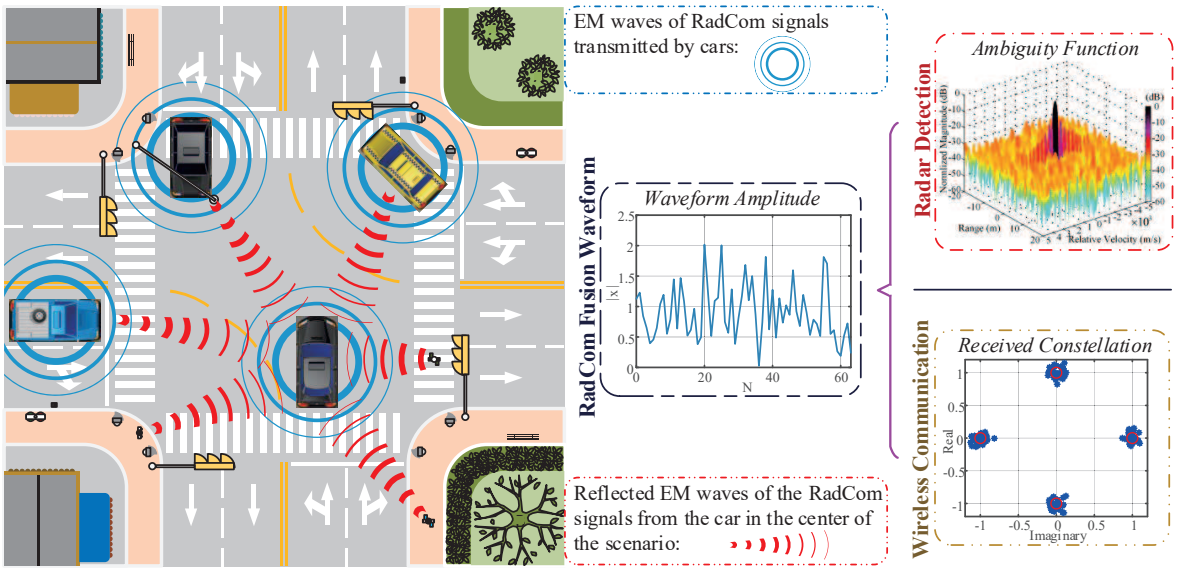

Fig. 1: An illustration of the communication and radar fusion system, i.e., RadCom, in an IoV scenario.

Specifically, low/zero periodic autocorrelation (PAC) property is highly required by OFDM-based RadCom systems. Spectrally-constrained sequences and the related correlation lower bounds have been derived in [12]. A unimodular sequence design algorithm has been developed in [13] through directly minimizing the integrated sidelobe level (ISL) with the aid of the majorization-minimization (MM) technique. Several algorithms based on the general MM method have been devised in [14] to tackle the weighted ISL and peak sidelobe level (PSL) minimization problem.

To deploy OFDM in a practical RadCom system, it is pivotal to reduce the peak-to-average power ratio (PAPR) of waveforms [15]. It is noted that traditional OFDM suffers from the high PAPR problem, which could result in serious nonlinear distortion of transmit signals incurred in a high power amplifier (HPA) of the radio frequency (RF) front end [17]. A PAPR-constrained Pareto-optimal waveform design approach has been proposed for low-PAPR OFDM radar waveform in [18]. OFDM waveforms with low autocorrelation and low PAPR have been derived under spectral constraints through the Gerchberg-Saxton (GS) algorithm in [19]. To reduce the PAPR of RadCom waveforms, a co-design OFDM waveform design based on a self-disarrange Golay block coding algorithm has been proposed in [20]. Furthermore, [21] investigated an OFDM-Chirp waveform which obtains PAPR about 6 dB lower than that of traditional OFDM. However, the data rates of these works may not be able to meet the communication rate requirements in practice. When a high-rate constraint is imposed in a RadCom system, in general, it is relatively difficult to achieve both good PAC characteristics and low PAPR.

B. Motivations and Objectives

Albeit extensive research efforts have been made on RadCom, a contiguous spectral band is mostly assumed in many existing RadCom systems. For sub-6 GHz bands, such a luxury has become very difficult to continue nowadays due to the increasingly congested and fragmented spectrum [22], [23]. Hence, there have been rapid advances on radar and communication systems operated over wideband millimeter-wave (mmWave) bands which provide relatively abundant spectrum resources. According to the *3GPP TS 38.104* standard, for example, mmWave communications can be conducted in the frequency range of 24.25-40 GHz and the specified bandwidths for 5G New Radio (NR) mmWave bands are 50 MHz, 100 MHz, 200 MHz and 400 MHz [24]. For excellent radar detection/sensing performance (e.g., good range resolution), in principle, the bandwidth allocated to a radar system, ranging from hundreds of megahertz to several gigahertz, may be far more larger than that for a traditional communication system.

In view of the increasingly congested and contiguous spectrum as well as different bandwidth requirements between communication and radar, a radical rethinking on the design of RadCom waveform structure with ultra flexibility in bandwidth allocation is becoming increasingly urgent. First, such a waveform design structure should allow radar to utilize contiguous or non-contiguous communication bands to increase the total detection bandwidth for enhanced range resolution. Second, the communication module can flexibly choose the desired transmission bandwidth and spectral locations based on its own quality-of-service requirements. With such a flexible waveform design structure, we aim for developing an OFDM-based RadCom system which can strike a balance between low-PAPR, sensing accuracy, and communication rates.

C. Problem Formulation and Contributions

We consider a generic OFDM-based RadCom waveform design structure where the communication bands lie at arbitrary positions of a large contiguous radar band (see Subsection II-A). Such a structure is highly flexible to

balance the different needs of radar and communication, where the former generally requires a large bandwidth for improved sensing resolution. We optimize the PAPR of the OFDM-based RadCom waveform over those bands which are complementary to the communication bands. When a low PAPR is required, for example, one may reduce the total communication bandwidth accordingly to reserve more bandwidth for RadCom waveform optimization. Also, one may allocate a larger bandwidth to communication when a high data rate is needed. The major contributions of this paper are summarized as follows:

- By observing that the short-range radar sensing/detection performance (e.g., range measurement) heavily relies on the PAC property of the waveform, we prove that the minimum period ISL (PISL) of the RadCom waveform is achieved when uniform power allocation is adopted for both radar and communication bands.
- Based on the proposed RadCom waveform structure, we propose a new efficient iterative waveform algorithm, called l-norm cyclic algorithm (LNCA), for effective PAPR reduction of OFDM-based RadCom waveforms by the general framework of the MM method.

It is found that the PAPR of the proposed RadCom waveform can be minimized by optimizing the infinite-norm (∞-norm) of energy spectrum of the oversampled waveforms (see Subsection III-B). Furthermore, we show that such an ∞-norm problem can be simplified by optimizing the associated l-norm, where l is a positive integer [14]. In the proposed algorithm, we first transform the l-norm problem associated to waveform energy spectrum into a quartic function problem by the MM method. Subsequently, the MM method is employed twice to transform the quartic function problem into a linear function optimization problem in Subsection IV-B. Thanks to the MM method, our proposed LNCA algorithm is guaranteed to converge and can be efficiently implemented by fast Fourier transform (FFT). In short, our proposed LNCA algorithm is capable of directly majorizing the maximum PAPR of OFDM-based RadCom waveforms in an effective manner for randomly distributed communication subcarriers.

D. Organization of this paper

This paper is organised as follow. The proposed generic RadCom waveform structure and the block diagram of OFDM-based RadCom systems are first introduced in Section II. The constraint and design objective of OFDM-based RadCom waveforms are shown in Section III. In Section IV, we show that optimized waveforms display PAPR of lower than 3 dB with a probability of higher than 99.99% by the proposed LNCA waveform, when the data bandwidth ratio[2] is 20%. To evaluate the performance of OFDM-based RadCom systems with the LNCA waveform, we present in Subsection V-A a set of 24 GHz ISM band-based mmWave system parameters to meet the demands of both the 5G NR and IoV radar. By taking a HPA at the RF front-end into account, we evaluate the performances of proposed low-PAPR waveforms in wireless communication and radar detection in Subsections V-B and V-C. Finally, we conclude this paper in Section VI.

[2]The data bandwidth ratio in this paper is defined as the communication bandwidth over the entire RadCom bandwidth.

Notations

The following notations will be used throughout this paper.

— $\mathrm{IDFT}(\cdot)$ and $\mathrm{DFT}(\cdot)$ denote inverse discrete Fourier transformation (IDFT) and discrete Fourier transformation (DFT) operations, respectively;
— $(\cdot)^{\mathrm{T}}$, $(\cdot)^{*}$ and $(\cdot)^{\mathrm{H}}$ denote the matrix transpose, conjugate and conjugate transpose operations, respectively;
— $(\mathbf{X} \cdot \mathbf{Y})$ denotes a Hadamard product of matrices or vectors, $\mathbf{X}$ and $\mathbf{Y}$;
— $\mathrm{Tr}(\cdot)$ denotes the matrix trace operation;
— $\mathrm{vec}(\cdot)$ denotes the matrix vectorization operation in column order;
— $\mathrm{diag}(\cdot)$ denotes a diagonal matrix formed with a vector as its principal diagonal;
— $\lambda_{\max}(\cdot)$ denotes the maximum matrix eigenvalue obtained from a matrix;
— $|\cdot|^2$ denotes the element-wise absolute-squared value;
— $\|\cdot\|$ denotes the Euclidean norm of a vector;
— $\|\cdot\|_l$ denotes the l-norm of a vector;
— $Q(x) = \int_x^\infty e^{-y^2/2}\, dy/\sqrt{2\pi}$ denotes the Gaussian Q-function.

II. OFDM-based RadCom Systems and Waveform Structure

Section II is a preparatory section in which we first introduce a generic OFDM-based RadCom waveform structure where the communication bands are allocated arbitrarily over a large contiguous radar band. Then we introduce a symbol-level OFDM-based RadCom system framework.

A. OFDM-based RadCom Waveform Structure

For compatibility with a wide range of spectrum usage patterns in both sub-6 GHz bands and mmWave bands, it is assumed throughout this paper that there are arbitrary number of (potentially non-contiguous) spectral bands which are used for communication purpose lying within a large contiguous radar band, as shown in Fig. 2. In this structure, the waveform PAPR can be reduced by optimizing those spectral bands (called "optimization band") complementary to the communication bands and the OFDM-based radar processing may be improved by adopting waveforms with the constraint of good PAC properties, which is shown in Subsection III-A.

Suppose that the set of all OFDM subcarriers is $\mathbf{\Omega} = \{0, 1, \ldots, N-1\}$, where N denote the number of subcarriers. Let $\mathbf{\Omega}^{\mathrm{c}}$ be the set of communication subcarrier indies with N_{c} as its cardinality. Also let $\mathbf{\Omega}^{\mathrm{d}}$ denote the set of subcarrier indices over which the PAC property and PAPR of the RadCom waveform is optimized, where N_{d} denotes its cardinality. Note that $N = N_{\mathrm{c}} + N_{\mathrm{d}}$, $\mathbf{\Omega}^{\mathrm{c}} \cup \mathbf{\Omega}^{\mathrm{d}} = \mathbf{\Omega}$ and $\mathbf{\Omega}^{\mathrm{c}} \cap \mathbf{\Omega}^{\mathrm{d}} = \mathbf{\Phi}_0$, where $\mathbf{\Phi}_0$ stands for the empty set. The communication symbol vector and the optimization symbol vector in discrete-frequency domain are defined as $\mathbf{C} \in \mathbb{C}^N$

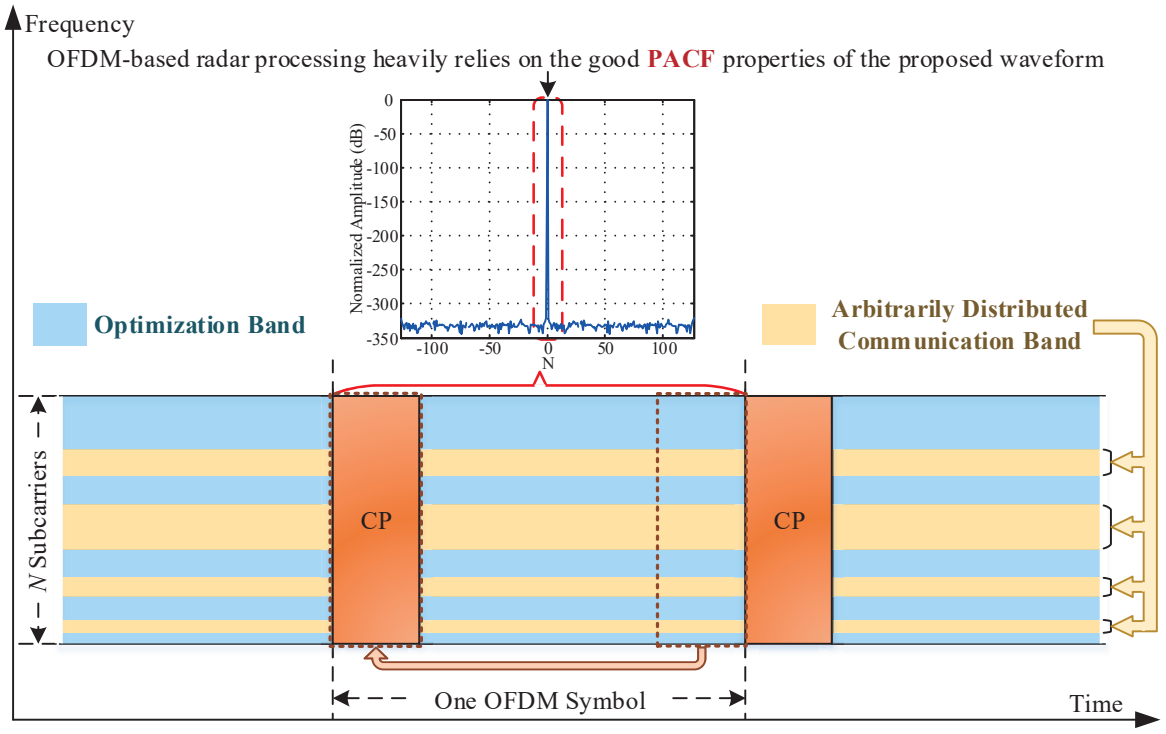

Fig. 2: Generic RadCom waveform structure in discrete-frequency domain.

and $\mathbf{D} \in \mathbb{C}^N$, respectively. It is noted that in any subcarrier position of $\mathbf{C}$ and $\mathbf{D}$, there is only one non-zero value, whilst the other one should be zero. The symbol vector in discrete-frequency domain is denoted as $\mathbf{X} = \mathbf{C} + \mathbf{D} = [X_0, X_1 \ldots, X_{N-1}]^{\mathrm{T}} \in \mathbb{C}^N$, and the element of $\mathbf{X}$ can be expressed as

$$X_k = \begin{cases} C_k, & \text{if } k \in \mathbf{\Omega}^{\mathrm{c}}, \\ D_k, & \text{otherwise}, \end{cases} \tag{1}$$

where C_k denotes the element of $\mathbf{C}$, D_k denotes the element of $\mathbf{D}$ and $k = 0, 1, \ldots, N-1$. The proposed waveform optimization is conducted over the N_{d} subcarriers.

B. OFDM-based RadCom System Structure

Based on the proposed waveform structure, the symbol-level signal processing flow in OFDM-based RadCom systems is depicted in Fig. 3, where the data bandwidth ratio is defined as $w = N_{\mathrm{c}}/N$. At the transmitter, without loss of generality, binary data are modulated by a phase shift keying (PSK) modulator to generate $\mathbf{C}$ and an unimodular sequence with random phases is used to generate $\mathbf{D}$ which will be optimized by the proposed waveform optimization algorithm in Section IV. The optimized $\mathbf{X}$ is then passed through an IDFT block module to generate the symbol vector in discrete-time domain, i.e., $\mathbf{x} = [x_0, x_1, \ldots, x_{N-1}]^{\mathrm{T}} \in \mathbb{C}^N$ and $\mathbf{x} = \mathrm{IDFT}(\mathbf{X})$. At last, the obtained $\mathbf{x}$ is passed through the cyclic prefix (CP) insertion and RF front end for transmission. For radar processing, the conjugate $\mathbf{X}$ is sent to generate a reference matrix in discrete-frequency domain. To calculate target range and relative velocity, let us assume that N_{f}, which denotes the number of evaluated OFDM symbols, symbols are needed. The element of the i-th symbol vector in discrete-time domain, i.e., $\mathbf{x}_i \in \mathbb{C}^N$, can be defined as

$$\begin{aligned} x_{i,n} &= \frac{1}{\sqrt{N}} \sum_{k=0}^{N-1} X_{i,k} e^{j2\pi \frac{kn}{N}}, \\ n &= 0, 1, \ldots, N-1, i = 0, 1, \ldots, N_{\mathrm{f}} - 1, \end{aligned} \tag{2}$$

where $X_{i,k}$ is the element of the i-th symbol vector in discrete-frequency domain, i.e., $\mathbf{X}_i = [X_{i,0}, X_{i,1}, \ldots, X_{i,N-1}]^{\mathrm{T}} \in \mathbb{C}^N$. The reference matrix is given by

$$\left[\mathbf{X}_0^* \quad \mathbf{X}_1^* \quad \ldots \quad \mathbf{X}_{N_{\mathrm{f}}-1}^*\right]. \tag{3}$$

At the receiver, after RF-level signal processing and CP removal, the received vector in discrete-time domain, defined as $\mathbf{y} \in \mathbb{C}^N$, is obtained. Then $\mathbf{y}$ is transformed by a DFT computation into the received vector in discrete-frequency domain, defined as $\mathbf{Y} = \mathrm{DFT}(\mathbf{y})$. According to the DFT result, i.e., $\mathbf{Y}$, the data in communication subcarriers will be extracted for PSK demodulation to get binary data and complete communication reception.

Let T_{sym}, T, T_{CP} and Δf be the total OFDM symbol duration, the OFDM symbol duration, the CP duration and the subcarrier spacing, respectively. We have $T_{\mathrm{sym}} = T + T_{\mathrm{CP}}$ and $T = 1/\Delta f$. In order to highlight the effect of delay and Doppler, let us ignore the noise. Assume that the OFDM radio waveforms are reflected by an object or obstacle in a certain range, calling L delays in a two-way propagation, with a Doppler shift $f_{\mathrm{D,rad}}$ due to a relative movement. Thus, the

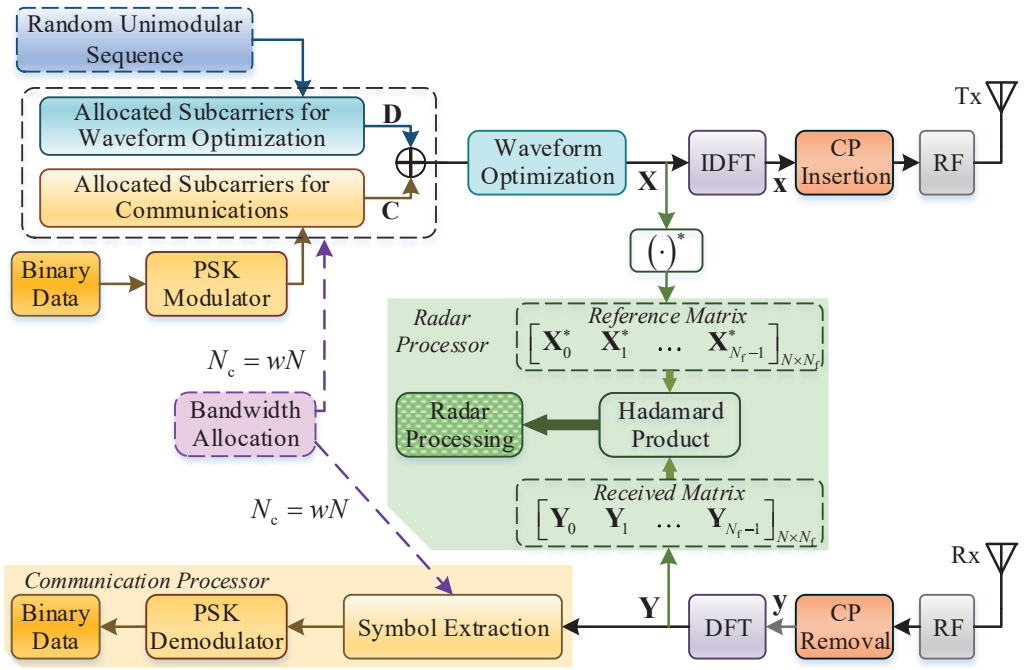

Fig. 3: Symbol-level signal processing block diagram of proposed OFDM-Based RadCom systems. The communication symbol vector, the optimization symbol vector, the symbol vector and the received vector in discrete-time domain, the symbol vector and the received vector in discrete-frequency domain are $\mathbf{C}$, $\mathbf{D}$, $\mathbf{x}$, $\mathbf{y}$, $\mathbf{X}$ and $\mathbf{Y}$, respectively. N, N_c, N_f and w are the number of subcarriers, the number of communication subcarriers, the number of evaluated OFDM symbols and the data bandwidth ratio, respectively.

element of the i-th received vector in discrete-time domain, i.e., $\mathbf{y}_i = [y_{i,0}, y_{i,1}, \dots, y_{i,N-1}]^{\mathrm{T}} \in \mathbb{C}^N$, can be written as [1]

$$\begin{aligned} y_{i,n} &= \frac{1}{\sqrt{N}} \sum_{k=0}^{N-1} Y_{i,k} e^{j2\pi \frac{kn}{N}} \\ &= \frac{1}{\sqrt{N}} \sum_{k=0}^{N-1} A_{i,k} X_{i,k} e^{-j2\pi \frac{kL}{N}} e^{j2\pi i f_{\mathrm{D,rad}} T_{\mathrm{sym}}} e^{j2\pi \frac{kn}{N}}, \\ n &= 0, 1, \dots, N-1, i = 0, 1, \dots, N_{\mathrm{f}} - 1, \end{aligned} \tag{4}$$

where $A_{i,k}$ denotes the complex amplitude factor describing the attenuation and phase shift occurring due to the propagation and scattering process, $Y_{i,k}$ is the element of the i-th received vector in discrete-frequency domain, i.e., $\mathbf{Y}_i = [Y_{i,0}, Y_{i,1}, \dots, Y_{i,N-1}]^{\mathrm{T}} \in \mathbb{C}^N$. Obviously, we have

$$\begin{aligned} Y_{i,k} &= A_{i,k} X_{i,k} e^{-j2\pi \frac{kL}{N}} e^{j2\pi i f_{\mathrm{D,rad}} T_{\mathrm{sym}}}, \\ k &= 0, 1, \dots, N-1, i = 0, 1, \dots, N_{\mathrm{f}} - 1. \end{aligned} \tag{5}$$

Let $\mathbf{k}_L = \left[1, e^{-j2\pi L/N}, \dots, e^{-j2\pi(N-1)L/N}\right]^{\mathrm{T}}$ and $\mathbf{A}_i = [A_{i,0}, A_{i,1}, \dots, A_{i,N-1}]^{\mathrm{T}}$, we have

$$\mathbf{Y}_i = e^{j2\pi i f_{\mathrm{D,rad}} T_{\mathrm{sym}}} \mathbf{A}_i \cdot \mathbf{X}_i \cdot \mathbf{k}_L, \ i = 0, 1, \dots, N_{\mathrm{f}} - 1. \tag{6}$$

The information about the objective is included in the symbol vectors and the received vectors in discrete-frequency domain, hence the N_{f} received vectors will be sent for constituting the received matrix in discrete-frequency domain, which can be written by

$$\left[\mathbf{Y}_0 \quad \mathbf{Y}_1 \quad \dots \quad \mathbf{Y}_{N_{\mathrm{f}}-1}\right]. \tag{7}$$

The radar processing algorithm used in this paper is based on a Hadamard product between the received matrix and the reference matrix. Then the typical OFDM radar processing [1] is adopted. Provided that the echo delay is shorter than the CP duration, the range can be calculated by exploiting the IDFT results of the Hadamard product of $\mathbf{X}^*$ and $\mathbf{Y}$, where the results are equivalent to the PAC function of $\mathbf{x}$ and $\mathbf{y}$. The Doppler shift is obtained by taking advantage of the DFT of samples on every subcarrier.

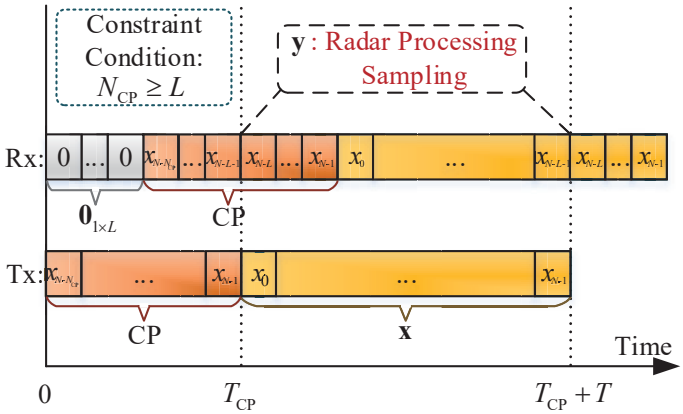

Fig. 4: The reflected echo diagram in time domain. T, T_{CP}, N_{CP} and L denote the OFDM symbol duration, the CP duration, the CP length and the maximum number of multi-paths, respectively. f_s stands for the sampling frequency which is equal to N/T . $\mathbf{x}$ and $\mathbf{y}$ are the symbol vector and the received vector in discrete-time domain, respectively.

III. OFDM-based RadCom Waveform: Constraint and Design Objective

In this section, we first introduce the optimization constraint and then formulate PAPR optimization objective function in OFDM-based RadCom waveform design. Since our objective is to optimize the PAPR of one symbol, the index i is ignored in the rest of this paper.

A. Optimization Constraint of RadCom Waveform

Consider an OFDM-based RadCom system, where N_{CP} and f_{s} denote the CP length and the sampling frequency, respectively. Obviously, $f_{\text{s}} = N/T$. In radar sensing/detection stage, as illustrated in Fig. 4, the OFDM symbol is reflected by a neighboring target and then the echo, which may be propagated through L delays, is received. When the attenuation of the transmit signal is ignored and $N_{\text{CP}} \geq L$, it is evident that $\mathbf{y}$ is a cyclic shift of $\mathbf{x}$, indicating that the ranging processing in the radar receiver can be equivalent to a periodic correlation function. Therefore, PAC properties of waveforms are significant for RadCom waveform design.

Formally, the PAC function (PACF) of $\mathbf{x}$ can be expressed as

$$r_{\mathbf{x}}(k) = \sum_{n=0}^{N-1} x_n x^*_{(n-k) \bmod N}, \tag{8}$$

where $k = -(N-1), \ldots, N-1$, and "mod" is the modulo operator. It is easy to find $r_{\mathbf{x}}(k) = r^*_{\mathbf{x}}(-k) = r^*_{\mathbf{x}}(N-k)$ at $k = 0, 1, \ldots, N-1$.

In OFDM radar signal processing, low/zero PACF sidelobes of the waveforms are preferred to prevent the masking effect[3]. It is noted that the power spectrum $\left\{|X_k|^2\right\}_{k=0}^{N-1}$ and $\{r_{\mathbf{x}}(k)\}_{k=0}^{N-1}$ form a Fourier transform pair [19]. The PISL of $\mathbf{x}$ can be written as [11]

$$\begin{aligned} \text{PISL} &= \sum_{\substack{k=-(N-1) \\ k\neq 0}}^{N-1} |r_{\mathbf{x}}(k)|^2 \\ &= 2\left(\sum_{k=0}^{N-1} |r_{\mathbf{x}}(k)|^2 - |r_{\mathbf{x}}(0)|^2\right) \\ &= 2\left(\sum_{k=0}^{N-1} \left(\sqrt{N}|X_k|^2\right)^2 - N^2\right) \\ &= 2\left(N\sum_{k=0}^{N-1} |X_k|^4 - N^2\right). \end{aligned} \tag{9}$$

Due to the Parseval's theorem and by assuming that $\sum_{n=0}^{N-1} |x_n|^2 = N$, we have $\sum_{k=0}^{N-1} |X_k|^2 = N$. One can easily show through the Cauchy-Schwarz inequality that the PISL can be minimized to zero by setting $|X_k| = 1,\ \forall\ k = 0,\ \ldots,\ N-1$. This indicates that when the elements of $\mathbf{X}$ are unimodular, the corresponding $\mathbf{x}$ has ideal PAC properties, i.e., PISL $= 0$. Hence, in OFDM-based RadCom systems with uniform power allocation, i.e., unimodular frequency samples, we consider the following settings as the constraint

$$\begin{cases} |X_k| = 1, & k \in \mathbf{\Omega}^{\text{d}}, \\ X_k = C_k, & k \in \mathbf{\Omega}^{\text{c}}, \end{cases} \tag{10}$$

where $|C_k| = 1, k \in \mathbf{\Omega}^c$ denote unimodular communication symbols, such as PSK symbols.

[3]The masking effect defined in this paper is that the target peak with weaker echo power is masked by the sidelobes of other targets.

B. Optimization Objectives of RadCom Waveform

Many radar systems require the waveform PAPR to be lower than 3 dB [18]. However, this may be hard to meet for OFDM systems, even using some traditional PAPR reduction methods (e.g., selected mapping, tone injection, tone reservation, etc.). It is widely believed that the PAPR of analog OFDM symbols can be very close to discrete OFDM symbols with four-times oversampling [15]. Based on this observation, for given $\mathbf{X} \in \mathbb{C}^N$, the elements of normalized four-times oversampled $\mathbf{x} \in \mathbb{C}^{4N}$ can be redefined as

$$x_n = \frac{1}{\sqrt{N}} \sum_{k=0}^{N-1} X_k e^{j2\pi \frac{kn}{4N}},\ n = 0, 1, \ldots, 4N-1. \tag{11}$$

The PAPR of a four-times oversampled OFDM symbol is defined as

$$\text{PAPR} = \frac{\max\limits_n \left\{|x_n|^2\right\}}{\frac{1}{4N}\sum\limits_{n=0}^{4N-1} |x_n|^2}. \tag{12}$$

For a given RadCom symbol vector in (10), $(1/4N)\sum_{n=0}^{4N-1} |x_n|^2 = 1$. Therefore, the PAPR optimization problem can be written as

$$\begin{aligned} &\min_{\mathbf{X}}\ \max_n\ \left\{\mathbf{X}^{\text{H}}\mathbf{a}_n\mathbf{a}_n^{\text{H}}\mathbf{X}\right\} \\ &s.t.\ \ |X_k| = 1, k \in \mathbf{\Omega}^{\text{d}}\ \text{ and }\ X_k = C_k, k \in \mathbf{\Omega}^{\text{c}}, \end{aligned} \tag{13}$$

where $\mathbf{a}_n = \frac{1}{\sqrt{N}}\left[1, e^{j2\pi\frac{n}{4N}}, \ldots, e^{j2\pi\frac{(N-1)n}{4N}}\right]^{\text{H}} \in \mathbb{C}^N$ and $x_n = \mathbf{a}_n^{\text{H}}\mathbf{X}$. This shows that the PAPR optimization in OFDM-based RadCom waveforms is equivalent to optimizing the ∞-norm of $|\mathbf{x}|^2$.

IV. Proposed l-Norm Cyclic Algorithms For PAPR Reduction In OFDM-based RadCom Systems

In this section, we introduce the MM method and then the proposed LNCA algorithm. Our key idea is to simplify the associated l-norm one which is then transformed into a linear optimization problem by employing the MM method for several times.

A. Majorization-Minimization Method

For minimization problem $f(\mathbf{x})$ over $\chi \in \mathbb{C}^N$, the MM method minimizes the objective function by optimizing an approximate function which majorizes $f(\mathbf{x})$. The function $u\left(\mathbf{x}, \mathbf{x}^{(q)}\right)$ is said to majorize $f(\mathbf{x})$ at point $\mathbf{x}^{(q)}$, where q in the superscript denotes the q-th iteration, provided that

$$u\left(\mathbf{x}, \mathbf{x}^{(q)}\right) \geq f(\mathbf{x}),\ \forall\ \mathbf{x} \in \chi, \tag{14}$$

$$u\left(\mathbf{x}^{(q)},\mathbf{x}^{(q)}\right)=f\left(\mathbf{x}^{(q)}\right). \tag{15}$$

It is clear that $u\left(\mathbf{x},\mathbf{x}^{(q)}\right)$ is an upper bound of $f(\mathbf{x})$ over χ and coincides with $f(\mathbf{x})$ at $\mathbf{x}^{(q)}$ [13]. Let $\mathbf{x}^{(q+1)}$ be the solution to $u\left(\mathbf{x},\mathbf{x}^{(q)}\right)$ at the $(q+1)$-th iteration, i.e., $\mathbf{x}^{(q+1)}\in \arg\min_{\mathbf{x}\in\chi} u\left(\mathbf{x},\mathbf{x}^{(q)}\right)$. One can see that the objective function decreases monotonically at every iteration, i.e.,

$$f\left(\mathbf{x}^{(q+1)}\right)\leq u\left(\mathbf{x}^{(q+1)},\mathbf{x}^{(q)}\right)\leq u\left(\mathbf{x}^{(q)},\mathbf{x}^{(q)}\right)=f\left(\mathbf{x}^{(q)}\right). \tag{16}$$

A simple and useful majorization result [13] is presented below:

Lemma 1: Let $\mathbf{M}\geq\mathbf{L}$, where $\mathbf{L}$ and $\mathbf{M}$ are $N\times N$ Hermitian matrices. Then for any point $\mathbf{x}_0\in\mathbb{C}^N$, the quadratic function $\mathbf{x}^{\mathrm{H}}\mathbf{L}\mathbf{x}$ is majorized by $\mathbf{x}^{\mathrm{H}}\mathbf{M}\mathbf{x}+2\,\mathrm{Re}\left(\mathbf{x}^{\mathrm{H}}\left(\mathbf{L}-\mathbf{M}\right)\mathbf{x}_0\right)+\mathbf{x}_0^{\mathrm{H}}\left(\mathbf{M}-\mathbf{L}\right)\mathbf{x}_0$ at $\mathbf{x}_0$.

B. l-Norm Cyclic Algorithm

In this subsection, we propose the LNCA algorithm for PAPR reduction over four-times oversampled RadCom waveforms. Since the ∞-norm optimization of a vector is not obvious, we consider the following l-norm optimization problem

$$\begin{aligned}&\min_{\mathbf{X}}\left(\sum_{n=0}^{4N-1}\left(\mathbf{X}^{\mathrm{H}}\mathbf{a}_n\mathbf{a}_n^{\mathrm{H}}\mathbf{X}\right)^l\right)^{\frac{1}{l}}\\&s.t.\ \ |X_k|=1,k\in\mathbf{\Omega}^{\mathrm{d}}\ \text{ and }\ X_k=C_k,k\in\mathbf{\Omega}^{\mathrm{c}},\end{aligned} \tag{17}$$

with $2\leq l<+\infty$. It is evident that the objective function of the above problem is the l-norm of $|\mathbf{x}|^2$. By choosing different l values, we may get different metrics of particular interest. For instance, by choosing $l\to+\infty$, the l-norm metric tends to the ∞-norm of $|\mathbf{x}|^2$ [14]. Therefore, the ∞-norm optimization problem in (13) can be converted into the l-norm optimization problem in (17) by choosing $l\to+\infty$. The above problem can be further simplified to

$$\begin{aligned}&\min_{\mathbf{X}}\sum_{n=0}^{4N-1}\left(\mathbf{X}^{\mathrm{H}}\mathbf{a}_n\mathbf{a}_n^{\mathrm{H}}\mathbf{X}\right)^l\\&s.t.\ \ |X_k|=1,k\in\mathbf{\Omega}^{\mathrm{d}}\ \text{ and }\ X_k=C_k,k\in\mathbf{\Omega}^{\mathrm{c}}.\end{aligned} \tag{18}$$

With the increase of l, the above l-norm optimization approaches to an ∞-norm optimization. Hence, this problem can be majorized with the aid of *Lemma 2* below [14]:

Lemma 2: Consider the l-th power function $f(x)=x^l$, where $l\geq 2$ and $x\in[0,t]$. Then, for any $x_0\in[0,t)$, $f(x)$ is majorized at x_0 over the interval $[0,t]$ by the following quadratic function

$$\alpha x^2+\left(lx_0^{l-1}-2\alpha x_0\right)x+\alpha x_0^2-(l-1)\,x_0^l, \tag{19}$$

where

$$\alpha=\frac{t^l-x_0^l-lx_0^{l-1}\left(t-x_0\right)}{\left(t-x_0\right)^2}. \tag{20}$$

By assuming $\mathbf{X}_q=\mathbf{X}^{(q)}$, which denotes the value of $\mathbf{X}$ at the q-th iteration, $\left(\mathbf{X}^{\mathrm{H}}\mathbf{a}_n\mathbf{a}_n^{\mathrm{H}}\mathbf{X}\right)^l$ is majorized at $\mathbf{X}_q^{\mathrm{H}}\mathbf{a}_n\mathbf{a}_n^{\mathrm{H}}\mathbf{X}_q$ over $[0,t]$ by

$$\begin{aligned}&\alpha_n\left(\mathbf{X}^{\mathrm{H}}\mathbf{a}_n\mathbf{a}_n^{\mathrm{H}}\mathbf{X}\right)^2+\beta_n\left(\mathbf{X}^{\mathrm{H}}\mathbf{a}_n\mathbf{a}_n^{\mathrm{H}}\mathbf{X}\right)\\&+\alpha_n\left(\mathbf{X}_q^{\mathrm{H}}\mathbf{a}_n\mathbf{a}_n^{\mathrm{H}}\mathbf{X}_q\right)^2-(l-1)\left(\mathbf{X}_q^{\mathrm{H}}\mathbf{a}_n\mathbf{a}_n^{\mathrm{H}}\mathbf{X}_q\right)^l,\end{aligned} \tag{21}$$

where

$$\begin{aligned}\alpha_n&=\frac{t^l-\left(\mathbf{X}_q^{\mathrm{H}}\mathbf{a}_n\mathbf{a}_n^{\mathrm{H}}\mathbf{X}_q\right)^l}{\left(t-\mathbf{X}_q^{\mathrm{H}}\mathbf{a}_n\mathbf{a}_n^{\mathrm{H}}\mathbf{X}_q\right)^2}-\frac{l\left(\mathbf{X}_q^{\mathrm{H}}\mathbf{a}_n\mathbf{a}_n^{\mathrm{H}}\mathbf{X}_q\right)^{l-1}}{t-\mathbf{X}_q^{\mathrm{H}}\mathbf{a}_n\mathbf{a}_n^{\mathrm{H}}\mathbf{X}_q},\\\beta_n&=l\left(\mathbf{X}_q^{\mathrm{H}}\mathbf{a}_n\mathbf{a}_n^{\mathrm{H}}\mathbf{X}_q\right)^{l-1}-2\alpha_n\mathbf{X}_q^{\mathrm{H}}\mathbf{a}_n\mathbf{a}_n^{\mathrm{H}}\mathbf{X}_q.\end{aligned} \tag{22}$$

As the objective function decreases at every iteration in MM optimization, $\sum_{n=0}^{4N-1}\left(\mathbf{X}^{\mathrm{H}}\mathbf{a}_n\mathbf{a}_n^{\mathrm{H}}\mathbf{X}\right)^l\leq\sum_{n=0}^{4N-1}\left(\mathbf{X}_q^{\mathrm{H}}\mathbf{a}_n\mathbf{a}_n^{\mathrm{H}}\mathbf{X}_q\right)^l$. Therefore, we choose $t=\left(\sum_{n=1}^{4N-1}\left(\mathbf{X}_q^{\mathrm{H}}\mathbf{a}_n\mathbf{a}_n^{\mathrm{H}}\mathbf{X}_q\right)^l\right)^{1/l}$. Since the constant term of the objective function does not affect the solution of the optimization problem, it can be ignored. By ignoring the constant terms of (21), the problem in (18) is majorized by

$$\begin{aligned}&\min_{\mathbf{X}}\sum_{n=0}^{4N-1}\left(\alpha_n\left(\mathbf{X}^{\mathrm{H}}\mathbf{a}_n\mathbf{a}_n^{\mathrm{H}}\mathbf{X}\right)^2+\beta_n\mathbf{X}^{\mathrm{H}}\mathbf{a}_n\mathbf{a}_n^{\mathrm{H}}\mathbf{X}\right)\\&s.t.\ \ |X_k|=1,k\in\mathbf{\Omega}^{\mathrm{d}}\ \text{ and }\ X_k=C_k,k\in\mathbf{\Omega}^{\mathrm{c}}.\end{aligned} \tag{23}$$

Thus, the l-norm problem in (18) is transformed into the quartic optimization problem in (23) by using *Lemma 2*. Then we have

$$\begin{aligned}&\sum_{n=0}^{4N-1}\left(\alpha_n\left(\mathbf{X}^{\mathrm{H}}\mathbf{a}_n\mathbf{a}_n^{\mathrm{H}}\mathbf{X}\right)^2+\beta_n\mathbf{X}^{\mathrm{H}}\mathbf{a}_n\mathbf{a}_n^{\mathrm{H}}\mathbf{X}\right)\\&=\sum_{n=0}^{4N-1}\left(\alpha_n\left(\mathbf{X}^{\mathrm{H}}\mathbf{a}_n\mathbf{a}_n^{\mathrm{H}}\mathbf{X}+\frac{\beta_n}{2\alpha_n}\right)^2-\frac{\beta_n^2}{4\alpha_n}\right)\\&=\sum_{n=0}^{4N-1}\left(\alpha_n\left(\mathbf{X}^{\mathrm{H}}\mathbf{a}_n\mathbf{a}_n^{\mathrm{H}}\mathbf{X}+\frac{\mathbf{X}^{\mathrm{H}}\mathbf{X}}{N}\cdot\frac{\beta_n}{2\alpha_n}\right)^2-\frac{\beta_n^2}{4\alpha_n}\right)\\&=\sum_{n=0}^{4N-1}\alpha_n\left(\mathbf{X}^{\mathrm{H}}\left(\mathbf{a}_n\mathbf{a}_n^{\mathrm{H}}+\frac{\beta_n}{2N\alpha_n}\mathbf{I}\right)\mathbf{X}\right)^2-\sum_{n=0}^{4N-1}\frac{\beta_n^2}{4\alpha_n}.\end{aligned} \tag{24}$$

In order to simplify the quadratic power terms of $\mathbf{X}^{\mathrm{H}}\left(\mathbf{a}_n\mathbf{a}_n^{\mathrm{H}}+\frac{\beta_n}{2N\alpha_n}\mathbf{I}\right)\mathbf{X}$, we let $\mathbf{\Phi}=\mathbf{X}\mathbf{X}^{\mathrm{H}}\in\mathbb{C}^{N\times N}$, $\zeta_n=\mathbf{a}_n\mathbf{a}_n^{\mathrm{H}}+\frac{\beta_n}{2N\alpha_n}\mathbf{I}\in\mathbb{C}^{N\times N}$, and we note that $\mathbf{X}^{\mathrm{H}}\left(\mathbf{a}_n\mathbf{a}_n^{\mathrm{H}}+\frac{\beta_n}{2N\alpha_n}\mathbf{I}\right)\mathbf{X}=\mathrm{Tr}(\mathbf{\Phi}\zeta_n)$. Since $\mathrm{Tr}(\mathbf{\Phi}\zeta_n)=\mathrm{vec}\left(\mathbf{\Phi}^{\mathrm{H}}\right)^{\mathrm{H}}\mathrm{vec}(\zeta_n)=\mathrm{vec}\left(\mathbf{\Phi}\right)^{\mathrm{H}}\mathrm{vec}(\zeta_n)$, by ignoring the constant terms of (24), we have

$$\begin{aligned}&\sum_{n=0}^{4N-1}\alpha_n\left|\mathrm{Tr}\left(\mathbf{\Phi}\zeta_n\right)\right|^2\\&=\sum_{n=0}^{4N-1}\alpha_n\,\mathrm{vec}\left(\mathbf{\Phi}\right)^{\mathrm{H}}\mathrm{vec}(\zeta_n)\,\mathrm{vec}\left(\zeta_n\right)^{\mathrm{H}}\mathrm{vec}(\mathbf{\Phi})\\&=\mathrm{vec}\left(\mathbf{\Phi}\right)^{\mathrm{H}}\left(\sum_{n=0}^{4N-1}\alpha_n\,\mathrm{vec}(\zeta_n)\,\mathrm{vec}\left(\zeta_n\right)^{\mathrm{H}}\right)\mathrm{vec}(\mathbf{\Phi})\\&=\mathrm{vec}\left(\mathbf{\Phi}\right)^{\mathrm{H}}\mathbf{L}\,\mathrm{vec}(\mathbf{\Phi}),\end{aligned} \tag{25}$$

where $\mathbf{L}=\sum_{n=0}^{4N-1}\alpha_n\,\mathrm{vec}(\zeta_n)\,\mathrm{vec}\left(\zeta_n\right)^{\mathrm{H}}\in\mathbb{C}^{N^2\times N^2}$. Hence, (23) can be simplified to

$$\begin{aligned}&\min_{\mathbf{\Phi}=\mathbf{X}\mathbf{X}^{\mathrm{H}}}\ \mathrm{vec}\left(\mathbf{\Phi}\right)^{\mathrm{H}}\mathbf{L}\,\mathrm{vec}(\mathbf{\Phi})\\&s.t.\ \ |X_k|=1,k\in\mathbf{\Omega}^{\mathrm{d}}\ \text{ and }\ X_k=C_k,k\in\mathbf{\Omega}^{\mathrm{c}}.\end{aligned} \tag{26}$$

Obviously, the optimization process is divided into two steps, where the first is in (23) and the second in (26). For given

$\mathbf{\Phi}_q = \mathbf{X}_q\mathbf{X}_q^{\mathrm{H}}$ and substituting $\mathbf{M} = \lambda_{\max}(\mathbf{L})\,\mathbf{I} \in \mathbb{C}^{N\times N}$ into *Lemma 1*, (26) can be majorized by the following function at $\mathbf{\Phi}_q$

$$\begin{aligned} u_1(\mathbf{\Phi},\mathbf{\Phi}_q) = & \lambda_{\max}(\mathbf{L})\,\mathrm{vec}(\mathbf{\Phi})^{\mathrm{H}}\mathrm{vec}(\mathbf{\Phi}) \\ & + 2\,\mathrm{Re}\Big(\mathrm{vec}(\mathbf{\Phi})^{\mathrm{H}}(\mathbf{L}-\lambda_{\max}(\mathbf{L})\,\mathbf{I})\,\mathrm{vec}(\mathbf{\Phi}_q)\Big) \\ & + \mathrm{vec}(\mathbf{\Phi}_q)^{\mathrm{H}}(\lambda_{\max}(\mathbf{L})\,\mathbf{I}-\mathbf{L})\,\mathrm{vec}(\mathbf{\Phi}_q). \end{aligned} \tag{27}$$

By ignoring the constant terms, we consider the following majorized problem

$$\begin{aligned} \min_{\mathbf{\Phi}=\mathbf{X}\mathbf{X}^{\mathrm{H}}} \ & \mathrm{Re}\left(\mathrm{vec}(\mathbf{\Phi})^{\mathrm{H}}(\mathbf{L}-\lambda_{\max}(\mathbf{L})\,\mathbf{I})\,\mathrm{vec}(\mathbf{\Phi}_q)\right) \\ s.t. \ & |X_k| = 1, k \in \mathbf{\Omega}^{\mathrm{d}} \ \text{ and } \ X_k = C_k, k \in \mathbf{\Omega}^{\mathrm{c}}. \end{aligned} \tag{28}$$

The quartic function problem in (23) has been converted to the quadratic optimization problem in (28) by applying *Lemma 1* first. Recalling the equivalent relationship in (25), the objective function in (28) can be rewritten as

$$\begin{aligned} & \mathrm{Re}\left(\mathrm{vec}(\mathbf{\Phi})^{\mathrm{H}}(\mathbf{L}-\lambda_{\max}(\mathbf{L})\,\mathbf{I})\,\mathrm{vec}(\mathbf{\Phi}_q)\right) \\ = & \mathrm{Re}\Big(\mathrm{vec}(\mathbf{\Phi})^{\mathrm{H}}\mathbf{L}\,\mathrm{vec}(\mathbf{\Phi}_q) - \lambda_{\max}(\mathbf{L})\mathrm{vec}(\mathbf{\Phi})^{\mathrm{H}}\mathbf{I}\,\mathrm{vec}(\mathbf{\Phi}_q)\Big) \\ = & \mathrm{Re}\left(\sum_{n=0}^{4N-1}\alpha_n\,\mathrm{vec}(\mathbf{\Phi})^{\mathrm{H}}\mathrm{vec}(\zeta_n)\,\mathrm{vec}(\zeta_n)^{\mathrm{H}}\mathrm{vec}(\mathbf{\Phi}_q) - \lambda_{\max}(\mathbf{L})\,\mathrm{vec}(\mathbf{\Phi})^{\mathrm{H}}\mathrm{vec}(\mathbf{\Phi}_q)\right) \\ = & \mathrm{Re}\left(\sum_{n=0}^{4N-1}\alpha_n\mathrm{Tr}(\zeta_n\mathbf{\Phi}_q)\mathrm{Tr}(\mathbf{\Phi}\zeta_n) - \lambda_{\max}(\mathbf{L})\mathrm{Tr}(\mathbf{\Phi}\mathbf{\Phi}_q)\right). \end{aligned} \tag{29}$$

Since $\mathbf{\Phi}$, $\mathbf{\Phi}_q$, ζ_n and $\mathbf{L}$ are conjugate symmetric matrices, the real part function $\mathrm{Re}(\cdot)$ can be omitted and $\mathrm{Tr}(\zeta_n\mathbf{\Phi}_q) = \mathrm{Tr}(\mathbf{\Phi}_q\zeta_n)$. Thus, (28) can be rewritten as

$$\begin{aligned} \min_{\mathbf{\Phi}=\mathbf{X}\mathbf{X}^{\mathrm{H}}} \ & \sum_{n=0}^{4N-1}\alpha_n\,\mathrm{Tr}(\mathbf{\Phi}_q\zeta_n)\,\mathrm{Tr}(\mathbf{\Phi}\zeta_n) - \lambda_{\max}(\mathbf{L})\,\mathrm{Tr}(\mathbf{\Phi}\mathbf{\Phi}_q) \\ s.t. \ & |X_k| = 1, k \in \mathbf{\Omega}^{\mathrm{d}} \ \text{ and } \ X_k = C_k, k \in \mathbf{\Omega}^{\mathrm{c}}. \end{aligned} \tag{30}$$

Noting that $\mathbf{X}^{\mathrm{H}}\left(\mathbf{a}_n\mathbf{a}_n^{\mathrm{H}} + \frac{\beta_n}{2N\alpha_n}\mathbf{I}\right)\mathbf{X} = \mathrm{Tr}(\mathbf{\Phi}\zeta_n)$, we have

$$\begin{aligned} & \sum_{n=0}^{4N-1}\alpha_n\,\mathrm{Tr}(\mathbf{\Phi}_q\zeta_n)\,\mathrm{Tr}(\mathbf{\Phi}\zeta_n) - \lambda_{\max}(\mathbf{L})\,\mathrm{Tr}(\mathbf{\Phi}\mathbf{\Phi}_q) \\ = & \sum_{n=0}^{4N-1}\alpha_n\mathrm{Tr}\left(\mathbf{X}_q\mathbf{X}_q^{\mathrm{H}}\left(\mathbf{a}_n\mathbf{a}_n^{\mathrm{H}} + \frac{\beta_n}{2N\alpha_n}\mathbf{I}\right)\right)\mathrm{Tr}\left(\mathbf{X}\mathbf{X}^{\mathrm{H}}\left(\mathbf{a}_n\mathbf{a}_n^{\mathrm{H}} + \frac{\beta_n}{2N\alpha_n}\mathbf{I}\right)\right) - \lambda_{\max}(\mathbf{L})\,\mathrm{Tr}\left(\mathbf{X}\mathbf{X}^{\mathrm{H}}\mathbf{X}_q\mathbf{X}_q^{\mathrm{H}}\right) \\ = & \sum_{n=0}^{4N-1}\alpha_n\mathbf{X}_q^{\mathrm{H}}\left(\mathbf{a}_n\mathbf{a}_n^{\mathrm{H}} + \frac{\beta_n}{2N\alpha_n}\mathbf{I}\right)\mathbf{X}_q\mathbf{X}^{\mathrm{H}}\left(\mathbf{a}_n\mathbf{a}_n^{\mathrm{H}} + \frac{\beta_n}{2N\alpha_n}\mathbf{I}\right)\mathbf{X} - \lambda_{\max}(\mathbf{L})\,\mathbf{X}^{\mathrm{H}}\mathbf{X}_q\mathbf{X}_q^{\mathrm{H}}\mathbf{X} \\ = & \sum_{n=0}^{4N-1}\alpha_n\left(\left|\mathbf{a}_n^{\mathrm{H}}\mathbf{X}_q\right|^2 + \frac{\beta_n}{2\alpha_n}\right)\left(\mathbf{X}^{\mathrm{H}}\mathbf{a}_n\mathbf{a}_n^{\mathrm{H}}\mathbf{X} + \frac{\beta_n}{2\alpha_n}\right) - \lambda_{\max}(\mathbf{L})\,\mathbf{X}^{\mathrm{H}}\mathbf{X}_q\mathbf{X}_q^{\mathrm{H}}\mathbf{X} \\ = & \sum_{n=0}^{4N-1}\alpha_n\left(\left|\mathbf{a}_n^{\mathrm{H}}\mathbf{X}_q\right|^2 + \frac{\beta_n}{2\alpha_n}\right)\mathbf{X}^{\mathrm{H}}\mathbf{a}_n\mathbf{a}_n^{\mathrm{H}}\mathbf{X} - \lambda_{\max}(\mathbf{L})\,\mathbf{X}^{\mathrm{H}}\mathbf{X}_q\mathbf{X}_q^{\mathrm{H}}\mathbf{X} + \sum_{n=0}^{4N-1}\frac{\beta_n}{2}\left(\left|\mathbf{a}_n^{\mathrm{H}}\mathbf{X}_q\right|^2 + \frac{\beta_n}{2\alpha_n}\right) \\ = & \frac{1}{2}\mathbf{X}^{\mathrm{H}}\left(2\sum_{n=0}^{4N-1}\mathbf{a}_n\alpha_n\left|\mathbf{a}_n^{\mathrm{H}}\mathbf{X}_q\right|^2\mathbf{a}_n^{\mathrm{H}} + \sum_{n=0}^{4N-1}\mathbf{a}_n\beta_n\mathbf{a}_n^{\mathrm{H}} - 2\lambda_{\max}(\mathbf{L})\,\mathbf{X}_q\mathbf{X}_q^{\mathrm{H}}\right)\mathbf{X} + \sum_{n=0}^{4N-1}\frac{\beta_n}{2}\left(\left|\mathbf{a}_n^{\mathrm{H}}\mathbf{X}_q\right|^2 + \frac{\beta_n}{2\alpha_n}\right). \end{aligned} \tag{31}$$

Furthermore, ignoring the constant term in (31), we have

$$\begin{aligned} & \mathbf{X}^{\mathrm{H}}\left(2\sum_{n=0}^{4N-1}\mathbf{a}_n\alpha_n\left|\mathbf{a}_n^{\mathrm{H}}\mathbf{X}_q\right|^2\mathbf{a}_n^{\mathrm{H}} + \sum_{n=0}^{4N-1}\mathbf{a}_n\beta_n\mathbf{a}_n^{\mathrm{H}} - 2\lambda_{\max}(\mathbf{L})\,\mathbf{X}_q\mathbf{X}_q^{\mathrm{H}}\right)\mathbf{X} \\ = & \mathbf{X}^{\mathrm{H}}\left(2\mathbf{A}^{\mathrm{H}}\mathrm{diag}(\alpha)\mathrm{diag}(\mathbf{p})\mathbf{A} + \mathbf{A}^{\mathrm{H}}\mathrm{diag}(\beta)\mathbf{A} - 2\lambda_{\max}(\mathbf{L})\,\mathbf{X}_q\mathbf{X}_q^{\mathrm{H}}\right)\mathbf{X} \\ = & \mathbf{X}^{\mathrm{H}}\left(\mathbf{A}^{\mathrm{H}}(2\mathrm{diag}(\alpha)\mathrm{diag}(\mathbf{p}) + \mathrm{diag}(\beta))\mathbf{A} - 2\lambda_{\max}(\mathbf{L})\,\mathbf{X}_q\mathbf{X}_q^{\mathrm{H}}\right)\mathbf{X}, \end{aligned} \tag{32}$$

where $\alpha = [\alpha_0, \alpha_1, \ldots, \alpha_{4N-1}]^{\mathrm{T}} \in \mathbb{C}^{4N}$, $\beta = [\beta_0, \beta_1, \ldots, \beta_{4N-1}]^{\mathrm{T}} \in \mathbb{C}^{4N}$, $\mathbf{A} = [\mathbf{a}_0, \mathbf{a}_1, \ldots, \mathbf{a}_{4N-1}]^{\mathrm{H}} \in \mathbb{C}^{4N\times N}$ denotes the four-times oversampling IDFT matrix, and $\mathbf{p} = |\mathbf{A}\mathbf{X}_q|^2 \in \mathbb{R}^{4N}$. Therefore, the problem in (30) can be rewritten as

$$\begin{aligned} \min_{\mathbf{X}} \ & \mathbf{X}^{\mathrm{H}}\left(\mathbf{A}^{\mathrm{H}}(2\mathrm{diag}(\alpha)\mathrm{diag}(\mathbf{p}) + \mathrm{diag}(\beta))\mathbf{A} - 2\lambda_{\max}(\mathbf{L})\,\mathbf{X}_q\mathbf{X}_q^{\mathrm{H}}\right)\mathbf{X} \\ s.t. \ & |X_k| = 1, k \in \mathbf{\Omega}^{\mathrm{d}} \ \text{ and } \ X_k = C_k, k \in \mathbf{\Omega}^{\mathrm{c}}. \end{aligned} \tag{33}$$

Let

$$\mathbf{\Gamma} = \mathbf{A}^{\mathrm{H}}(2\,\mathrm{diag}(\alpha)\mathrm{diag}(\mathbf{p}) + \mathrm{diag}(\beta))\mathbf{A} - 2\lambda_{\max}(\mathbf{L})\mathbf{X}_q\mathbf{X}_q^{\mathrm{H}} \tag{34}$$

and

$$\begin{aligned} \mathbf{M} = \gamma\mathbf{A}^{\mathrm{H}}\mathbf{A} \geq & \mathbf{A}^{\mathrm{H}}\left(2\,\mathrm{diag}(\alpha)\,\mathrm{diag}(\mathbf{p}) + \mathrm{diag}(\beta)\right)\mathbf{A} \\ & - 2\lambda_{\max}(\mathbf{L})\,\mathbf{X}_q\mathbf{X}_q^{\mathrm{H}}, \end{aligned} \tag{35}$$

where $\mathbf{\Gamma}, \mathbf{M} \in \mathbb{C}^{N\times N}$ and $\gamma = \max_n\{2\alpha_n p_n + \beta_n\}$, $n = 0, 1, \ldots, 4N-1$. Therefore, the problem in (33) can be majorized by

$$u_2(\mathbf{X},\mathbf{X}_q) = \gamma\mathbf{X}^{\mathrm{H}}\mathbf{A}^{\mathrm{H}}\mathbf{A}\mathbf{X} + 2\mathrm{Re}\left(\mathbf{X}^{\mathrm{H}}(\mathbf{\Gamma}-\mathbf{M})\,\mathbf{X}_q\right) + \mathbf{X}_q^{\mathrm{H}}(\mathbf{M}-\mathbf{\Gamma})\mathbf{X}_q. \tag{36}$$

Note that $(\mathbf{\Gamma}-\mathbf{M})$ is a Hermitian matrix. Ignoring the constant terms of (36), the optimization function can be

translated to

$$\begin{aligned} &\min_{\mathbf{X}} \ \mathbf{X}^{\mathrm{H}}\left(\mathbf{\Gamma}-\mathbf{M}\right)\mathbf{X}_q \\ &s.t. \ \ |X_k|=1, k\in\mathbf{\Omega}^{\mathrm{d}} \ \text{ and } \ X_k=C_k, k\in\mathbf{\Omega}^{\mathrm{c}}. \end{aligned} \tag{37}$$

The quadratic problem in (28) has been simplified to a linear one in (37) by adopting *Lemma 1*.

According to the orthogonality theorem, it is easy to get

$$\begin{aligned} \|\mathbf{X}-\mathbf{Y}_\Delta\|^2 &= \left(\mathbf{X}-\mathbf{Y}_\Delta\right)^{\mathrm{H}}\left(\mathbf{X}-\mathbf{Y}_\Delta\right) \\ &= \left(\mathbf{X}^{\mathrm{H}}-\mathbf{Y}_\Delta^{\mathrm{H}}\right)\left(\mathbf{X}-\mathbf{Y}_\Delta\right) \\ &= \mathbf{X}^{\mathrm{H}}\mathbf{X}-\left(\mathbf{Y}_\Delta^{\mathrm{H}}\mathbf{X}+\mathbf{X}^{\mathrm{H}}\mathbf{Y}_\Delta\right)+\mathbf{Y}_\Delta^{\mathrm{H}}\mathbf{Y}_\Delta \\ &= \|\mathbf{X}\|^2+\|\mathbf{Y}_\Delta\|^2+2\,\mathrm{Re}\left(\mathbf{X}^{\mathrm{H}}\left(-\mathbf{Y}_\Delta\right)\right) \\ &= \|\mathbf{X}\|^2+\|\mathbf{Y}_\Delta\|^2+2\mathrm{Re}\big(\mathbf{X}^{\mathrm{H}}(\mathbf{\Gamma}-\mathbf{M})\mathbf{X}_q\big), \end{aligned} \tag{38}$$

where $\mathbf{Y}_\Delta = -\left(\mathbf{\Gamma}-\mathbf{M}\right)\mathbf{X}_q$. Omitting the constant terms in (38), i.e., $\|\mathbf{X}\|^2$ and $\|\mathbf{Y}_\Delta\|^2$, the problem in (37) can be rewritten as

$$\begin{aligned} &\min_{\mathbf{X}} \ \|\mathbf{X}-\mathbf{Y}_\Delta\| \\ &s.t. \ \ |X_k|=1, k\in\mathbf{\Omega}^{\mathrm{d}} \ \text{ and } \ X_k=C_k, k\in\mathbf{\Omega}^{\mathrm{c}}. \end{aligned} \tag{39}$$

Since $2\lambda_{\max}(\mathbf{L})\mathbf{X}_q\mathbf{X}_q^{\mathrm{H}}\mathbf{X}_q=2N\lambda_{\max}(\mathbf{L})\mathbf{X}_q=\frac{N}{2}\lambda_{\max}(\mathbf{L})\mathbf{A}^{\mathrm{H}}\mathbf{A}\mathbf{X}_q$, we have

$$\begin{aligned} &\mathbf{Y}_\Delta = -\left(\mathbf{\Gamma}-\mathbf{M}\right)\mathbf{X}_q \\ &=-\big(\mathbf{A}^{\mathrm{H}}(2\mathrm{diag}(\alpha)\mathrm{diag}(\mathbf{p})+\mathrm{diag}(\beta)-\gamma\mathbf{I})\mathbf{A}-2\lambda_{\max}(\mathbf{L})\mathbf{X}_q\mathbf{X}_q^{\mathrm{H}}\big)\mathbf{X}_q \\ &=-\mathbf{A}^{\mathrm{H}}\left(2\mathrm{diag}(\alpha)\mathrm{diag}(\mathbf{p})+\mathrm{diag}(\beta)-\gamma\mathbf{I}-\frac{N}{2}\lambda_{\max}(\mathbf{L})\mathbf{I}\right)\mathbf{A}\mathbf{X}_q. \end{aligned} \tag{40}$$

Since $\frac{N}{2}\lambda_{\max}\left(\mathbf{L}\right)\mathbf{I}$ is sufficiently smaller than $2\,\mathrm{diag}(\alpha)\,\mathrm{diag}(\mathbf{p})+\mathrm{diag}(\beta)-\gamma\mathbf{I}$, $\frac{N}{2}\lambda_{\max}\left(\mathbf{L}\right)\mathbf{I}$ can be omitted in (40). The above equation can be rewritten as

$$\mathbf{Y}_\Delta=-\mathbf{A}^{\mathrm{H}}\left(2\,\mathrm{diag}(\alpha)\,\mathrm{diag}(\mathbf{p})+\mathrm{diag}(\beta)-\gamma\mathbf{I}\right)\mathbf{A}\mathbf{X}_q. \tag{41}$$

Assuming that $Y_k, k=0,1,\ldots,N-1$ denotes the element of $\mathbf{Y}_\Delta$, the proposed algorithm based on l-norm is summarized in Table I.

Under the same waveform structure, the waveform PAPR can also be optimized by a traditional GS method [19], [25], [26] and a typical MM Method [14], which are referred to in this paper as the partially-reserved GS (PRGS) algorithm and the partially-reserved MM (PRMM) algorithm, respectively. The partially-reserved OFDM (PROFDM), which uses the communication bands for data transmission while power normalized random symbols[4] are transmitted in the optimization bands, is also considered for comparison. The complementary cumulative distribution function (CCDF) PAPR performances of the four-times oversampled PROFDM, PRGS, PRMM and LNCA waveforms are compared in Fig. 5 with randomly distributed communication subcarriers. It is observed that the PAPR of each waveform grows as w increases. For a given w, the best PAPR performance is always obtained by the proposed LNCA waveform, followed by the PRMM and PRGS waveforms. In particular, when CCDF $= 0.01\%$ and $w = 0.2$, our proposed LNCA waveform achieves a PAPR of at most 3 dB, which is 9 dB lower than that of the PROFDM waveform. One can see that the PAPR of RadCom waveforms can be effectively reduced by the proposed LNCA algorithm with randomly distributed communication subcarriers. As will be shown in the next section, this can effectively reduce the nonlinear distortion of HPAs and hence greatly improve the power transmission efficiency.

[4]A random symbol in this paper is defined as a complex symbol where its real part and imaginary part obey the standard normal distribution.

TABLE I: Proposed LNCA Algorithm

Step 0: Consider l and $q=0$. Store transmit data $\mathbf{C}: C_k,\ k\in\mathbf{\Omega}^c$, generate an initial optimization vector $\mathbf{D}^{(q)}: D_k^{(q)}=e^{j\theta_k},\ k\in\mathbf{\Omega}^d$, where θ_k is randomly selected in $[0,2\pi]$. Then, generate an initial RadCom symbol vector in discrete-frequency domain $\mathbf{X}_q=\mathbf{C}+\mathbf{D}^{(q)}$.
Step 1: For fixed $\mathbf{X}_q$, compute $\mathbf{X}_{\mathrm{t}}=\mathbf{A}\mathbf{X}_q$, $\mathbf{p}=|\mathbf{X}_{\mathrm{t}}|^2$ and $t=\|\mathbf{p}\|_l$.
Step 2: For fixed $\mathbf{p}$ and t, compute

$$\alpha_n=\frac{t^l-p_n^l-lp_n^{l-1}\left(t-p_n\right)}{\left(t-p_n\right)^2},$$

$$\beta_n=lp_n^{l-1}-2\alpha_n p_n,$$

$$\gamma=\max_n\left\{2\alpha_n p_n+\beta_n\right\},$$

where $n=0,1,\ldots,4N-1$.
Step 3: For fixed α_n, β_n and γ, update

$$\mathbf{Y}_\Delta=-\mathbf{A}^{\mathrm{H}}\left(2\,\mathrm{diag}(\alpha)\,\mathrm{diag}(\mathbf{p})+\mathrm{diag}(\beta)-\gamma\mathbf{I}\right)\mathbf{A}\mathbf{X}_q.$$

Step 4: For fixed $\mathbf{Y}_\Delta$, update

$$D_k^{(q+1)}=\exp\left(j\arg(Y_k)\right),\ k\in\mathbf{\Omega}^d.$$

Then $\mathbf{X}_{q+1}=\mathbf{C}+\mathbf{D}^{(q+1)}$ and $q=q+1$.
Iteration: Repeat **Step 1** to **Step 4**, until a stopping criteria is met, e.g., $q\geq 50$.

V. Performance Evaluation For OFDM-based RadCom Systems

To evaluate performance of both wireless communication and radar detection/sensing with the proposed LNCA waveform, we first present a set of 24 GHz ISM band-based RadCom system parameters in this section. Taking randomly distributed communication subcarriers, the solid-state power amplifier (SSPA) and input-back-off (IBO) into consideration, we then evaluate the OFDM-based RadCom system performances, where the bit error rate (BER) performance is for wireless communication and the target detection performances, including the ambiguity function, the radar image and the detection probability are for radar.

A. Parameters for OFDM-based RadCom Systems

In the case of the radar application with relative velocity v between radar transceiver and targets, the Doppler shift of echoes at the receiver is [27]

$$f_{\mathrm{D,rad}}=\frac{2v}{\lambda}=\frac{2vf_{\mathrm{c}}}{c}, \tag{42}$$

where c denotes the speed of light, λ the wavelength and f_{c} the carrier frequency. It is noted that a communication signal goes through a one-way propagation whereas a radar

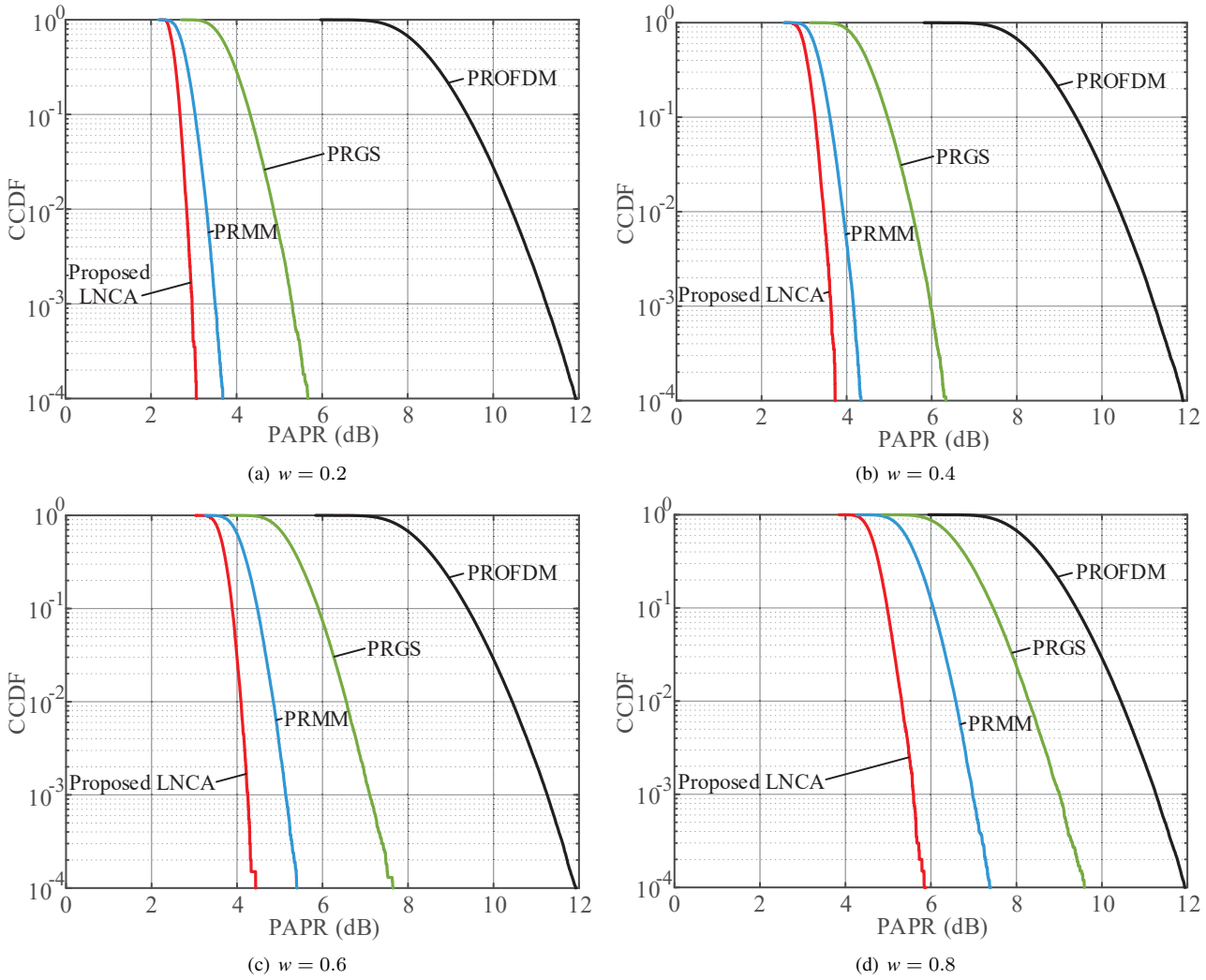

(a) $w = 0.2$ (b) $w = 0.4$

(c) $w = 0.6$ (d) $w = 0.8$

Fig. 5: CCDF comparison for the PAPRs of different four-times oversampled waveforms with randomly distributed communication subcarriers.

TABLE II: Parameters of OFDM-based RadCom systems with randomly distributed communication subcarriers

Symbol	Parameter	Value
f_c	Carrier frequency	24 GHz
N	Number of subcarriers	4096
Δf	Subcarrier spacing	60 kHz
T	OFDM symbol duration	16.67 μs
T_{CP}	Cyclic prefix duration	1.33 μs
T_{sym}	Total OFDM symbol duration	18 μs
B	Signal bandwidth	245.76 MHz
ΔR	Radar range resolution	0.61 m
R_{max}	Maximum range, limited by T_{CP}	200 m
Δv	Radar velocity resolution	1.36 m/s
v_{max}	Maximum relative velocity, limited by Δf	75 m/s
N_{f}	Number of evaluated symbols	256
w	Data bandwidth ratio	0.2

transmission undergoes a two-way propagation. The Doppler shift of transmit signals at the communication receiver is [28]

$$f_{\text{D,com}} = \frac{v}{\lambda} = \frac{v f_c}{c}. \tag{43}$$

Hence, the Doppler shift experienced by the communication module is half of that of radar, i.e. $f_{\text{D,com}} = f_{\text{D,rad}}/2$.

In Table II, a complete set of 24 GHz ISM band-based parameters for OFDM-based RadCom systems which may be deployed in both IoV and 5G NR. According to *3GPP TS 38.104*, 50 MHz is the narrowest band and 60 kHz is smallest subcarrier spacing in standard mmWave frequency bands of 5G NR [24]. With regard to this, Δf is set to be 60 kHz and $T = 1/\Delta f \approx 16.67$ μs.

For reliable information exchange in OFDM systems, it is desired that the maximum Doppler shift $f_{\text{D,com,max}}$ should be smaller than $0.1\Delta f$ in order to combat with the intercarrier interference [1], i.e. $f_{\text{D,com,max}} = 0.5 f_{\text{D,rad,max}} < 0.1\Delta f$. To satisfy requirements of classical traffic scenario, a relative velocity of up to 200 km/h and a range of maximum 200 m are considered. Since $\Delta f = 60$ kHz, $f_{\text{D,com,max}} = 6$ kHz and $f_{\text{D,rad,max}} = 12$ kHz, the maximum relative velocity is $v_{\text{max}} = 75$ m/s (i.e., 270 km/h) according to (42). T_{CP} is set to 1.33 μs to meet the ideal maximum range of 200 m, i.e., $R_{\text{max}} = 200$ m, and the maximum multipath delay of 400 m.

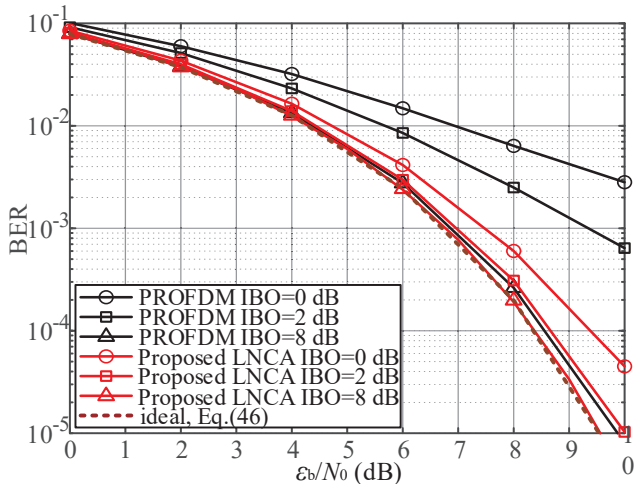

Fig. 6: BER comparison of OFDM-based RadCom systems in AWGN channel by SSPA. $w = 0.2$ with randomly distributed communication subcarriers.

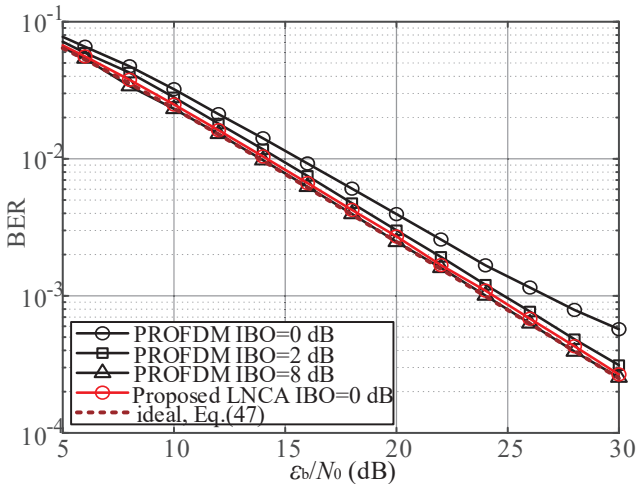

Fig. 7: BER comparison of OFDM-based RadCom systems in Rayleigh channel by SSPA. $w = 0.2$ with randomly distributed communication subcarriers.

Hence, $T_{\text{sym}} = T + T_{\text{CP}} = \ 18\ \mu$s. N is set to 4096, which results in the signal bandwidth $B = 245.76$ MHz and radar range resolution $\Delta R = 0.61$ m. N_{f} is set to 256 that leads to radar velocity resolution $\Delta v = 1.36$ m/s. Moreover, w is set to 0.2 and the communication subcarriers are distributed randomly.

In the Rapp model of SSPA, the input signal is $s_{\text{in}} = A_{\text{in}} e^{j\varphi_{\text{in}}}$, where A_{in} and φ_{in} denote amplitude and phase, respectively. The output signal is $s_{\text{out}} = G\left(A_{\text{in}}\right) e^{j[\varphi_{\text{in}} + \Phi(A_{\text{in}})]}$, where $G\left(\cdot\right)$ and $\Phi\left(\cdot\right)$ denote the AM/AM conversion and AM/PM conversion of SSPA, respectively. According to [29], we have

$$\begin{cases} G\left(A_{\text{in}}\right) = \dfrac{g_0 A_{\text{in}}}{\left[1 + \left(A_{\text{in}}/A_{\text{sat}}\right)^{2p}\right]^{1/2p}}, \\ \Phi\left(A_{\text{in}}\right) = 0, \end{cases} \tag{44}$$

where g_0 stands for the amplifier gain, A_{sat} the saturation level of SSPA and the index p the smoothness parameter on the transition smoothness from the linear region to the saturated region. To reduce the signal nonlinear distortion at the RadCom transmitter, the IBO operation, which reduces the power of input signals, is applied. Here, the IBO is defined as [29]

$$\text{IBO} = \frac{A_{\text{sat}}^2}{P_{\text{in}}}, \tag{45}$$

where P_{in} is the input average power of SSPA. Roughly speaking, an IBO value equal to the waveform PAPR guarantees the transmit signal is linearly amplified in SSPA without nonlinear distortion [30]. In this paper, we assume $g_0 = 1$, $A_{\text{sat}} = 1$ and $p = 2$.

B. Performance Evaluation of Communication Performances in RadCom

Since quadrature PSK (QPSK) symbols are transmitted in communication band, their signal processing is the same as that for traditional OFDM systems. Therefore, in additive white gaussian noise (AWGN) channel, the BER of OFDM-based RadCom systems with the proposed LNCA waveform can be expressed as [31]

$$\text{BER}_{\text{AWGN}} \approx 2\left(\frac{\sqrt{M}-1}{\sqrt{M}\log_2\sqrt{M}}\right) Q\left(\sqrt{\frac{3\log_2 M}{M-1}\frac{\varepsilon_{\text{b}}}{N_0}}\right), \tag{46}$$

where $\varepsilon_{\text{b}} = wA^2T/(N\log_2 M)$ denotes the energy per bit of received signals, A the signal amplitude, M the PSK modulation order and N_0 the power spectral density (PSD) of AWGN. In Rayleigh channel, the BER performance of an OFDM-based RadCom system with the proposed LNCA waveform is expressed as [32]

$$\text{BER}_{\text{Ray}} \approx \frac{c_1}{2}\left(1 - \sqrt{\frac{c_2^2\varepsilon_{\text{b}}/N_0}{2 + c_2^2\varepsilon_{\text{b}}/N_0}}\right), \tag{47}$$

where $c_1 = 2\left(\sqrt{M}-1\right)/\left(\sqrt{M}\log_2\sqrt{M}\right)$, $c_2 = \sqrt{3\log_2 M/(M-1)}$.

For $w = 0.2$ with randomly distributed communication subcarriers, Fig. 6 compares the BER performance of OFDM-based RadCom with the proposed LNCA and PROFDM waveforms when the transmit waveforms are amplified by SSPA. With a minimum mean-squared error (MMSE) equalizer [25], the BER performances of such an OFDM based RadCom system in Rayleigh channel are shown in Fig. 7. In AWGN channel, the BER of the proposed waveforms (called "LNCA waveforms") at IBO $= 2$ dB is similar to that of PROFDM at IBO $= 8$ dB, both of which are close to the ideal BER performance. In Rayleigh channel, the BER of the LNCA waveforms at IBO $= 0$ dB is close to the ideal performance in which PROFDM requires IBO $= 8$ dB.

C. Performance Evaluation of Target Detection in RadCom

The ambiguity function of a transmit waveform in continuous-time domain, i.e. $x\left(t\right),\ t \in (-\infty, \infty)$, is defined as [11]

$$\chi\left(\tau, f_{\text{D,rad}}\right) = \int_{-\infty}^{\infty} x\left(t\right) x^*\left(t-\tau\right) e^{j2\pi f_{\text{D,rad}} t} dt. \tag{48}$$

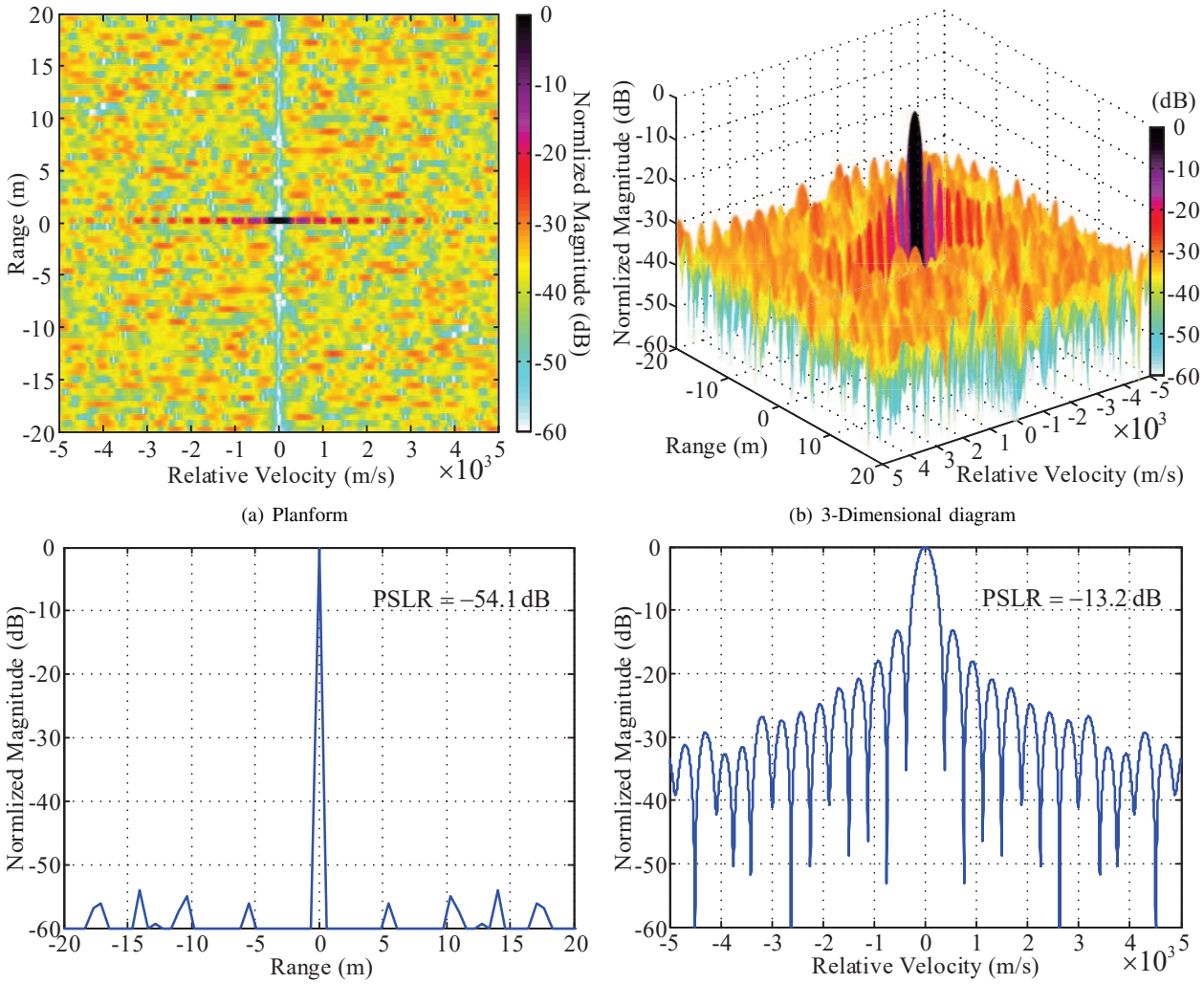

(a) Planform

(b) 3-Dimensional diagram

(c) Range profile with relative velocity of 0 m/s

(d) Relative velocity profile with range of 0 m

Fig. 8: Ambiguity function of one proposed LNCA waveform.

Fig. 8(a) and Fig. 8(b) show the ambiguity function of one LNCA waveform from the planform and the 3D perspectives, respectively. Targets may be distinguished if the relative range/velocity between targets is larger than the range/velocity ambiguity, which depends on the width of the main peak. In Fig. 8(c), the range ambiguity is about 0.6 m and the PSL ratio (PSLR) is -54.1 dB, where the former is consistent with ΔR in Table II and the latter helps prevent the masking effect. In Fig. 8(d), the detection with one LNCA waveform suffers a velocity ambiguity of about 370 m/s PSLR of -13.2 dB. Due to the undesired velocity ambiguity of a single LNCA waveform, 256 symbols are required to make Δv approach to 1.36 m/s in Table II.

Due to the two-way propagation for radar transmission, the power of reflected echoes is denoted as follows [1]:

$$P_{\mathrm{Rx}} = \frac{P_{\mathrm{Tx}} G_{\mathrm{Tx}} G_{\mathrm{Rx}} \sigma_{\mathrm{RCS}} \lambda^2}{(4\pi)^3 R^4}, \tag{49}$$

where P_{Tx} denotes the power of transmit waveforms, G_{Tx} the transmitter gain, G_{Rx} the receiver gain, σ_{RCS} the radar cross section of target and R the distance between target and radar receiver. In an OFDM-based RadCom system, the gain provided by radar processing is equal to the number of correlated samples [1]. In the case of processing over N_{f} symbols each consisting of N subcarriers, this unique processing results in a total processing gain of

$$G_{\mathrm{P}} = N N_{\mathrm{f}}. \tag{50}$$

The signal-to-noise ratio (SNR) of radar image can be obtained when thermal noise power, P_{N}, and receiver noise figure, N_{Fig},

TABLE III: Typical Radar Parameters of a Practical Implementation [1]

Symbol	Value	Parameter
f_{c}	24 GHz	Carrier frequency
$P_{\mathrm{Tx}} G_{\mathrm{Tx}}$	12.73 dBm	24 GHz ISM limit 12.73 dBm EIRP [33]
P_{N}	-90 dBm	Thermal noise for 250 MHz
N_{Fig}	6 dB	System noise figure
$\sigma_{\mathrm{RCS,min}}$	-10 dBm^2	Worst case RCS
G_{Rx}	20 dBi	HPBW 45° AZ, 9° EL
$\mathrm{SNR}_{\mathrm{image,min}}$	10 dB	Worst radar image SNR
G_{P}	60.2 dB	NN_{f}, OFDM processing gain

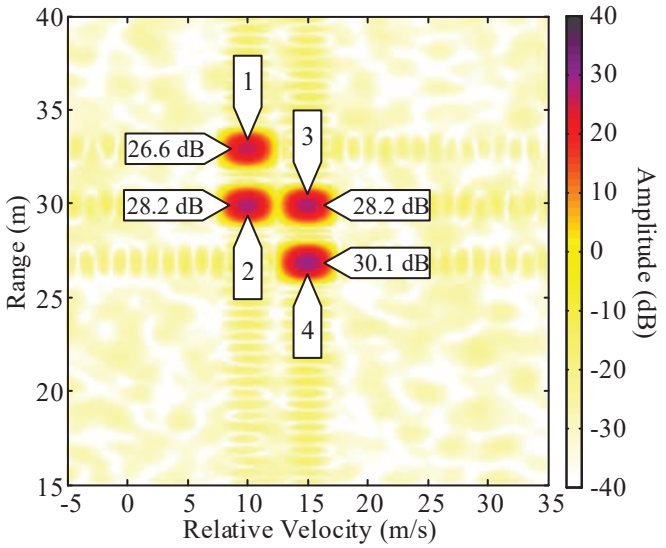

(a) The proposed LNCA waveform

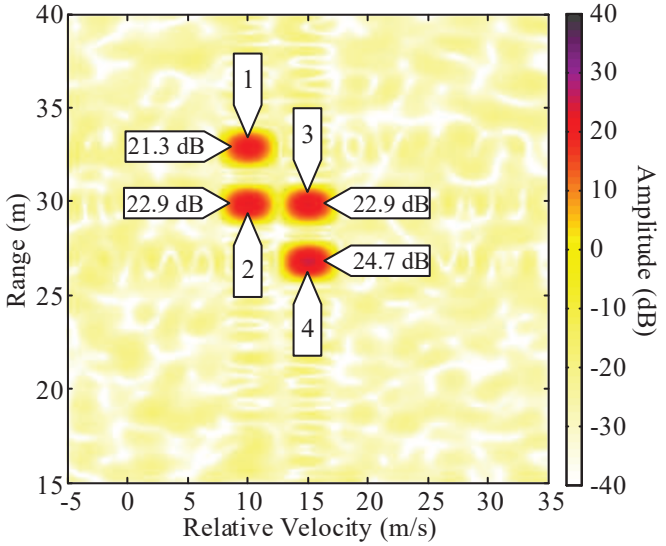

(b) The PROFDM waveform

Fig. 9: Radar images for four targets with $w = 0.2$ and arbitrarily distributed communication subcarriers. Normalized to $\sigma_{\text{RCS}} = 0$ dBm^2 and $R = 10$ m.

are taken into account [1]

$$\text{SNR}_{\text{image}} = \frac{P_{\text{Rx}} G_{\text{P}}}{P_{\text{N}} N_{\text{Fig}}}. \tag{51}$$

Taking additionally into account (49), we have

$$\text{SNR}_{\text{image}} = \frac{P_{\text{Tx}} G_{\text{Tx}} N N_{\text{f}} G_{\text{Rx}} \sigma_{\text{RCS}} \lambda^2}{P_{\text{N}} N_{\text{Fig}} (4\pi)^3 R^4}. \tag{52}$$

From (52) and radar parameters in Table III, the maximum range for radar application can be calculated to be 140.5 m.

The plots of the radar images with the proposed LNCA and PROFDM waveforms are depicted in Fig. 9 according to the four point scatterers and parameters in Table IV. These radar images are obtained on the condition of $G_{\text{Tx}} = 20$ dB, $G_{\text{Rx}} = 20$ dBi, $\sigma_{\text{RCS}} = 24$ dBm^2, $w = 0.2$, QPSK modulation and $\text{SNR}_{\text{image}} = 60.2$ dB. And these images are normalized

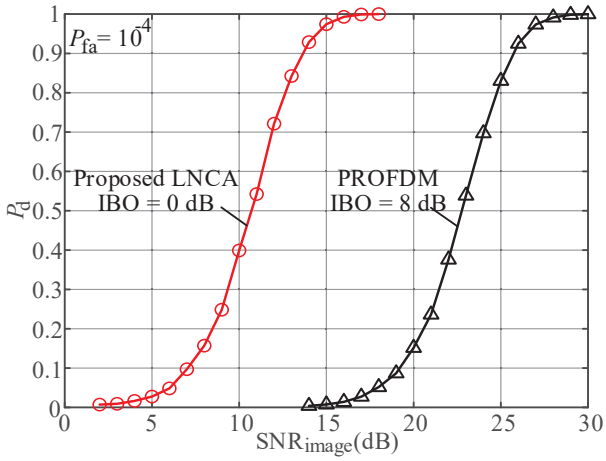

Fig. 10: Detection probability by the proposed LNCA and PROFDM waveforms with $P_{\text{fa}} = 10^{-4}$. Detection for single target with $R = 30$ m and $v \in (-v_{\max}, +v_{\max})$.

to $\sigma_{\text{RCS}} = 0$ dBm^2 and $R = 10$ m. It is clear that these four targets can be distinguished in Fig. 9(a) and Fig. 9(b) whilst the LNCA waveform leads to a gain of at least 5.3 dB in every target peak comparing to the PROFDM waveform.

TABLE IV: Range and Relative Velocity of Four Targets

Target	Range (m)	Relative Velocity (m/s)
1	33	10
2	30	10
3	30	15
4	27	15

In order to further evaluate the detection performance of the RadCom system with the LNCA waveforms, a two-dimensional constant false alarm rate (CFAR) detector is used in Fig. 10 on the basis of the Neyman-Pearson criterion and the parameters in Table III. The detection probability and false alarm probability are defined as P_{d} and P_{fa}, respectively. For detecting single target with $R = 30$ m and $v \in (-v_{\max}, +v_{\max})$, Fig. 10 displays detection probabilities associated to the LNCA waveforms with IBO $= 0$ dB and the PROFDM waveform with IBO $= 8$ dB when $P_{\text{fa}} = 10^{-4}$. The P_{d} of the LNCA waveforms increases with $\text{SNR}_{\text{image}}$ in 3-18 dB when that of the PROFDM waveform increases with $\text{SNR}_{\text{image}}$ in 14-30 dB. Compared to PROFDM with IBO $= 8$ dB, the required $\text{SNR}_{\text{image}}$ of the LNCA waveform with IBO $= 0$ dB leads a gain of 12 dB to obtain the same P_{d} by CFAR. This gain is achieved due to the low PAPR properties of the LNCA waveforms, which lead to enhanced radar detection probability performance.

VI. Conclusions

In this paper, we have introduced a new waveform design algorithm, i.e. LNCA, to reduce PAPR of OFDM-based RadCom waveforms by considering a flexible and generic RadCom waveform structure. Our proposed LNCA algorithm benefits from a key observation that the waveform PAPR optimization problem can be transformed into an ∞-norm one whose simplified expression implies that a low-PAPR

waveform is possible provided that a special cyclic phase transform in optimization band gives rise to a low PAPR. With the aid of MM method, we further show that the ∞-norm problem can be simplified as an linear function optimization problem. Thanks to the obtained low-PAPR and perfect PAC properties, our numerical simulations show that the proposed LNCA waveforms give rise to enhanced HPA efficiency and detection probability in OFDM-based RadCom systems. Two interesting future directions are 1) to design optimal beam patterns in OFDM-MIMO based RadCom systems [3] and 2) to improve our proposed algorithm with a one step majorization and by taking into account of some coding or nonlinear signal processing techniques.

ACKNOWLEDGMENT

The authors are deeply indebted to the anonymous Reviewers for many of their insightful comments which have greatly helped improve the quality of this work. This work is partially supported by the National Natural Science Foundation of China (No. 61971092), Sichuan Province Foundation for Distinguished Young Scholars (No. 2020JDJQ0023), and the Fundamental Research Funds for the Central Universities (No. ZYGX2020ZB045, No. ZYGX2019J123), ERA-NET Smart Energy Systems SG+ 2017 Program, "SMART-MLA" with Project number 89029 (and SWEA number 42811-2), and FORMAS project entitled "Intelligent Energy Management in Smart Community with Distributed Machine Learning", number 2021-00306, and Swedish Research Council Project entitled "Coding for Large-scale Distributed Machine Learning", number 2021-04772.

REFERENCES

[1] C. Sturm and W. Wiesbeck, "Waveform design and signal processing aspects for fusion of wireless communications and radar sensing," *Proc. IEEE*, vol. 99, no. 7, pp. 1236-1259, Jul. 2011.

[2] S. H. Dokhanchi, B. S. Mysore, K. V. Mishra, and B. Ottersten, "A mmWave automotive joint radar-communications system," *IEEE Trans. on Aero. Elec. Sys.*, vol. 55, no. 3, pp. 1241-1260, Jun. 2019.

[3] F. Liu, C. Masouros, A. Li, H. Sun and L. Hanzo, "MU-MIMO communications with MIMO radar: from co-existence to joint transmission," *IEEE Trans. Wireless Commun.*, vol. 17, no. 4, pp. 2755-2770, Apr. 2018.

[4] S. Hu, B. Yu, C. Qian, Y. Xiao, Q. Xiong, C. Sun, and Y. Gao, "Nonorthogonal interleave-grid multiple access scheme for industrial internet of things in 5G network," *IEEE Trans. Ind. Inform.*, vol. 14, no. 12, pp. 5436-5446, Jul. 2018.

[5] J. F. Gu, J. Moghaddasi, and K. Wu, "Delay and Doppler shift estimation for OFDM-based radar-radio (RadCom) system," in *Proc. IEEE Int. Wireless Symp. (IWS)*, Mar. 2015, pp. 1-4.

[6] J. R. Krier *et al*., "Performance bounds for an OFDM-based joint radar and communications system," in *Proc. IEEE Mil. Commun. Conf. (Milcom)*, Oct. 2015, pp. 511-516.

[7] X. Tian and Z. Song, "On radar and communication integrated system using OFDM signal," in *Proc. IEEE Radar Conf. (RadarConf)*, May 2017, pp. 318-323.

[8] Y. Liu, G. Liao, J. Xu, Z. Yang, and Y. Zhang, "Adaptive OFDM integrated radar and communications waveform design based on information theory," *IEEE Commun. Lett.*, vol. 21, no. 10, pp. 2174-2177, Jul. 2017.

[9] C. Shi, F. Wang, M. Sellathurai, J. Zhou, and S. Salous, "Power minimization based robust OFDM radar waveform design for radar and communication systems in coexistence," *IEEE Trans. Signal Process.*, vol. 66, no. 5, pp. 1316-1330, Nov. 2017.

[10] F. Liu, L. Zhou, C. Masouros, A. Li, W. Luo and A. Petropulu, "Toward dual-functional radar-communication systems: optimal waveform design," *IEEE Trans. Signal Process.*, vol. 66, no. 16, pp. 4264-4279, Aug. 2018.

[11] H. He, J. Li, and P. Stoica, *Waveform Design for Active Sensing Systems - A Computational Approach*. New York: Cambridge University Press, 2012. pp: 17-19 & 88-97.

[12] Z. Liu, Y. L. Guan, U. Parampalli, and S. Hu, "Spectrally-constrained sequences: bounds and constructions," *IEEE Trans. Inform. Theory*, vol. 64, no. 4, pp. 2571-2582, Apr. 2018.

[13] J. Song, P. Babu, and D. P Palomar, "Optimization methods for designing sequences with low autocorrelation sidelobes," *IEEE Trans. Signal Process.*, vol. 63, no. 15, pp. 3998-4009, Apr. 2015.

[14] J. Song, P. Babu, and D. P. Palomar, "Sequence design to minimize the weighted integrated and peak sidelobe levels," *IEEE Trans. Signal Process.*, vol. 64, no. 8, pp. 2051-2064, Apr. 2016.

[15] S. H. Han and J. H. Lee, "An overview of peak-to-average power ratio reduction techniques for multicarrier transmission," *IEEE Wireless Commun.*, vol. 12, no. 2, pp. 56-65, Apr. 2005.

[16] Y. Huang, S. Hu, S. Ma, Q. Luo, D. Huang, Y. Gao, and R. Shi, "Constant envelope OFDM RadCom fusion system," *Eurasip JWCN*, May 2018.

[17] Y. Yang, J. Mei, D. Hu, Y. Lei, and X. Luo, "Research on reducing PAPR of QAM-OFDM radar-communication integration sharing signal," in *IET Int. Radar Conf. (IRC 2018)*, Oct. 2018, pp. 8042-8046.

[18] S. Sen, "PAPR-constrained pareto-optimal waveform design for OFDM-STAP Radar," *IEEE Trans. Geosci. Remote Sensing*, vol. 52, no. 6, pp. 3658-3669, Jun. 2014.

[19] L.-S. Tsai, W.-H. Chung and D.-S. Shiu, "Synthesizing low autocorrelation and low PAPR OFDM sequences under spectral constraints through convex optimization and GS algorithm," *IEEE Trans. Signal Process.*, vol. 59, no. 5, pp. 1055-1065, May 2011.

[20] W. Li, P. Ren, and Z. Xiang, "Waveform design for dual-function radar-communication system with golay block coding," *IEEE Access*, vol. 7, pp. 184053 - 184062, Dec. 2019.

[21] W. Jia, W. Q. Wang, Y. Hou, and S. Zhang, "Integrated communication and localization system With OFDM-Chirp waveform," *IEEE Systems Journal*, vol. 14, no. 2, pp. 2464 - 2472, Jun. 2019.

[22] Z. Liu, Y. L. Guan, S. Hu, and U. Parampalli, "Optimal spectrally-constrained sequences," in *Proc. IEEE Int. Symp. Inform. Theory (ISIT)*, Jun. 2015, pp. 2692-2696.

[23] Y. Huang, D. Huang, Q. Luo, S. Ma, S. Hu, and Y. Gao , "NC-OFDM RadCom system for electromagnetic spectrum interference," in *Proc. IEEE 17th Int. Conf. Commun. Techn. (ICCT)*, Oct. 2017, pp. 877-881.

[24] Technical Specification Group Radio Access Network; NR; Base Stations (BS) Radio Transmission and Reception (Release 15), document *3GPP TS 38.104 V15.5.0*, 3rd Generation Partnership Project, Mar. 2019. [Online]. Available: https://www.3gpp.org/DynaReport/38-series.htm

[25] S. Hu, Z. Liu, Y. L. Guan, W. Xiong, G. Bi, and S. Li, "Sequence design for cognitive CDMA communications under arbitrary spectrum hole constraint," *IEEE J. Select. Areas Commun.*, vol. 32, no. 11, pp. 1974-1986, Dec. 2014.

[26] H. He, P. Stoica, and J. Li, "Unimodular sequence sets with good correlations for MIMO radar," in *Proc. 2009 IEEE Radar Conf. Pasadena*, CA, 2009, pp. 1-6.

[27] F. Gini, A. D. Maio and L. K Patton, *Waveform Design and Diversity for Advanced Radar Systems*. London, UK: The Institution of Engineering and Technology, 2012, pp. 5-7.

[28] Y. S. Cho, J. Kim, W. Y. Yang and C. G. Kang, *MIMO-OFDM Wireless Communications with MATLAB*. Singapore: John Wiley & Sons (Asia) Pte Ltd, 2010, pp. 19-24.

[29] C. Rapp, "Effects of HPA-nonlinearity on a 4-DPSK/OFDM signal for a digital sound broadcasting system," in *Proc. IEEE 56th Veh. Techn. Conf. (VTC)*, Oct. 1991, pp. 179-184.

[30] H. Ochiai, "Performance analysis of peak power and band-limited OFDM system with linear scaling," *IEEE Trans. Wireless Commun.*, vol. 2, no. 5, pp. 1055-1065, Sep. 2003.

[31] K. Cho and D. Yoon, "On the general BER expression of one- and two-dimensional amplitude modulations," *IEEE Trans. Commun.*, vol. 50, no. 7, pp. 1074-1080, Jul. 2002.

[32] M. K. Simon and M.-S. Alouini, *Digital Communication over Fading Channels*. 1st ed., New York, USA: John Wiley & Sons, Inc., 2000, pp. 101-101.

[33] Understanding the FCC regulations for low-power, non-licenced transmitters, document *FCC OET Bulletin 63*, Federal Communications Commission, Oct. 1993. [Online]. Available: https://www.fcc.gov/general/oet-bulletins-line

Yixuan Huang received his B.S. degree in Yingcai Honers College from the University of Electronic Science and Technology of China (UESTC), China, in 2015. He was a postgraduate student from 2015 to 2017, and has been a Ph.D candidate from 2017 in the National Key Laboratory of Science and Technology on Communication, UESTC, China. His main fields of research interest include broadband multicarrier wireless communication system and detection and communication (RadCom) integrative waveform design.

Su Hu received his Master and PhD. degree in National Key Lab of Communication from University of Electronic Science and Technology of China (UESTC), Chengdu, China, in 2007 and 2010, respectively. Currently, he is a full professor in UESTC. His research areas include waveform design of multicarrier systems, cognitive radio, and signal processing in wireless communication system.

Shiyong Ma Shiyong Ma received his B.S. and M.S. degree from the University of Electronic Science and Technology of China, Chengdu, China, in 2017 and in 2020, respectively. His research interests include wireless communication, waveform design, and integrated communication and radar system.

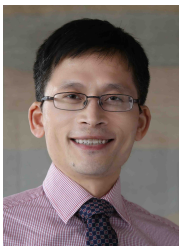

Zilong Liu is a Lecturer (Assistant Professor) at the School of Computer Science and Electronic Engineering, University of Essex. He received his PhD (2014) from School of Electrical and Electronic Engineering, Nanyang Technological University (NTU, Singapore), Master Degree (2007) in the Department of Electronic Engineering from Tsinghua University (China), and Bachelor Degree (2004) in the School of Electronics and Information Engineering from Huazhong University of Science and Technology (HUST, China). From Jan. 2018 to Nov. 2019, he was a Senior Research Fellow at the Institute for Communication Systems (ICS), Home of the 5G Innovation Centre (5GIC), University of Surrey, during which he studied the air-interface design of 5G communication networks (e.g., machine-type communications, V2X communications, 5G New Radio). Prior to his career in UK, he spent nine and half years in NTU, first as a Research Associate (Jul. 2008 to Oct. 2014) and then a Research Fellow (Nov. 2014 to Dec. 2017). His PhD thesis Perfect- and Quasi- Complementary Sequences, focusing on fundamental limits, algebraic constructions, and applications of complementary sequences in wireless communications, has settled a few long-standing open problems in the field. His research lies in the interplay of coding, signal processing, and communications, with a major objective of bridging theory and practice as much as possible. He is a Senior Member of IEEE and an Associate Editor of IEEE Wireless Communications Letters, IEEE Access, and Frontiers in Communications and Networks. He is/was a General Co-Chair of the 2022 International Workshop on Signal Design and its Applications in Communications (IWSDA2022) and a TPC Co-Chair of the 2020 IEEE International Conference on Advanced Networks and Telecommunications Systems (ANTS2020). He was a tutorial speaker of VTC-Fall2021 and APCC2021 on code-domain NOMA. Besides, he was/is a TPC member of a number of IEEE Conferences/Workshops (e.g., ICC, GLOBECOM, WCSP, ICCS, SETA). So far, he has published over 100 peer-reviewed journal/conference papers with more than 40 IEEE Transactions papers. Details of his research can be found at: https://sites.google.com/site/zilongliu2357.

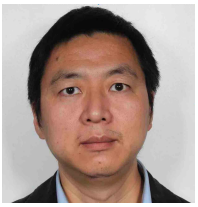

Ming Xiao (S'2002-M'2007-SM'2012) received Bachelor and Master degrees in Engineering from the University of Electronic Science and Technology of China, ChengDu in 1997 and 2002, respectively. He received Ph.D degree from Chalmers University of technology, Sweden in November 2007. From 1997 to 1999, he worked as a network and software engineer in ChinaTelecom. From 2000 to 2002, he also held a position in the SiChuan communications administration. From November 2007 to now, he has been in the department of information science and engineering, school of electrical engineering and computer science, Royal Institute of Technology, Sweden, where he is currently an Associate Professor. He was an Editor for IEEE Transactions on Communications (2012-2017), IEEE Communications Letters (Senior Editor Since January 2015) and IEEE Wireless Communications Letters (2012-2016), and has been an Editor for IEEE Transactions on Wireless Communications since 2018. He has been an area editor for IEEE Open Journal of the Communication Society since 2019.